[American Journal of Science, Vol. 314, January, 2014, P. 314–356, DOI 10.2475/01.2014.09]

PLUME-LITHOSPHERE INTERACTION IN THE GENERATION OF THE TARIM LARGE IGNEOUS PROVINCE, NW CHINA: GEOCHRONOLOGICAL AND GEOCHEMICAL CONSTRAINTS

XUN WEI*,**, YI-GANG XU*,†, YUE-XING FENG***, and JIAN-XIN ZHAO***

ABSTRACT. The magmatism in the early Permian Tarim large igneous province (TLIP) in NW China is represented by basaltic lava flows in Keping and ultramafic-mafic-felsic intrusions and mafic dikes in Bachu, northwestern Tarim Craton. This paper reports new Ar-Ar dating results and chemical compositions of Keping basalts and Bachu dikes, with aims of better characterizing the timing of and mantle/crustal contribution to the TLIP. The Keping basalts yield two well-defined $^{40}Ar/^{39}Ar$ plateau ages of 287.3 ± 4.0 Ma and 287.9 ± 4.1 Ma, which, together with age data from the literature, define a magmatic event at ~289 Ma. The intrusions and dikes in Bachu are believed to have formed at ~279 Ma based on screened literature data. Thus, they together define two magmatic episodes. The Keping basalts, representing the earlier episode, have alkaline affinity (SiO_2 = 44.0-47.9 wt.%, $Na_2O + K_2O$ = 3.7-4.9 wt.%), low MgO (4.3-5.9 wt.%) and high TiO_2 (3.8-5.1 wt.%) contents, showing fractionated chondrite-normalized LREE and nearly flat HREE patterns [$(La/Yb)_N$ = 6.27-7.71; $(Dy/Yb)_N$ = 1.36-1.48] with noticeable negative Nb and Ta anomalies in the primitive mantle-normalized trace element diagram. They have negative and relatively uniform $\varepsilon_{Nd}(t)$ (−2.3 to −3.8) and low $(^{206}Pb/^{204}Pb)_i$ (17.43-17.57). We argue that these "crustal signatures" cannot be attributed to crustal assimilation because neither $\varepsilon_{Nd}(t)$ nor $(^{206}Pb/^{204}Pb)_i$ correlates with SiO_2; rather they are more likely derived from a sub-continental lithospheric mantle (SCLM) source metasomatized by subduction-related processes. The Bachu dikes, representing the later episode and confined to the margins of the Tarim Craton, have similar MgO (3.6-5.4 wt.%) and TiO_2 (3.1-4.7 wt.%) contents to the Keping basalts, and display more fractionated REE patterns [$(La/Yb)_N$ = 10.1-14.0; $(Dy/Yb)_N$ = 1.79-1.99]. They have variable isotope compositions [$\varepsilon_{Nd}(t)$ = −0.3-4.8, $(^{206}Pb/^{204}Pb)_i$ = 17.50-18.11] and display OIB-like trace element signatures. Correlations between isotopic and trace element ratios indicate that some dikes with low $\varepsilon_{Nd}(t)$ and low initial Pb isotope ratios could have been subjected to crustal assimilation. We propose a model involving plume-lithosphere interaction to account for the two discrete magmatic episodes with distinct mantle sources in the TLIP. The earlier episode was formed in response to the impact of a sub-lithospheric mantle plume at the base of the SCLM. Partial melting of the metasomatized lithospheric mantle was triggered by temperature increase due to conductive heating of the impregnating mantle plume. The later episode was generated by decompression melting of the mantle plume, as a result of deflection of the plume towards the margins of the Tarim Craton with thinner lithosphere.

Key words: Tarim large igneous province, $^{40}Ar/^{39}Ar$ dating, Keping basalts, Bachu dikes, lithosphere-mantle plume interaction, plume deflection

INTRODUCTION

Large Igneous Provinces (LIPs) occur as a result of widespread ($>10^5$ km^2) and voluminous ($>10^5$ km^3) mafic magmatism which, together with minor associated felsic and silica-undersaturated alkaline components, have a maximum lifespan of ~50 Ma and are characterized by igneous pulses of short duration (1-5 Ma) (Bryan and Ernst,

* State Key Laboratory of Isotope Geochemistry, Guangzhou Institute of Geochemistry, Chinese Academy of Sciences, Guangzhou 510640, China
** University of Chinese Academy of Sciences, Beijing 100049, China
*** Radiogenic Isotope Facility, School of Earth Sciences, The University of Queensland, Brisbane, QLD 4072, Australia
† Corresponding author: yigangxu@gig.ac.cn

2008). They are often associated with the arrival of deep mantle plumes at the base of the lithosphere (Richards and others, 1989, 1991; Campbell and Griffiths, 1990; Griffiths and Campbell, 1990; Hill and others, 1992; Courtillot and others, 2003; He and others, 2003; Xu and others, 2004a; Campbell, 2005; Wolfe and others, 2009). The Permian is an important period in the earth's history, and is characterized by the emplacement of two well-known LIPs including the ~251 Ma Siberian Traps in Russia (Campbell and others, 1992; Lightfoot and others, 1993; Arndt and others, 1998; Reichow and others, 2002, 2009) and the ~260 Ma Emeishan LIP in SW China (Chung and Jahn, 1995; Xu and others, 2001, 2004a; Zhou and others, 2002). The early Permian volcanic rocks and intrusions are also abundant in the Tarim Craton, NW China and they represent another Permian LIP (Yang and others, 2007; Bryan and Ernst, 2008; Zhang and others, 2008a; Tian and others, 2010). Understanding the mechanism and geodynamic processes that were responsible for the formations of these LIPs will contribute significantly to the understanding of mantle geochemistry and mantle plumes.

The early Permian Tarim LIP (TLIP) in northwest China covers an area of more than 250,000 km^2 and consists of predominant basaltic lava flows, ultramafic-mafic-felsic layered intrusions, felsic volcanic rocks and dikes, mainly outcropping in Keping, Bachu and Damusi areas in the western Tarim Craton (Chen and others, 1997a; Jiang and others, 2004; Yang and others, 2006b, 2007; Li and others, 2008; Zhang and others, 2008a, 2010b, 2010c; Zhou and others, 2009; Tian and others, 2010; Yu and others, 2011b). The formation of the TLIP has been attributed to a mantle plume (Pirajno and others, 2008; Zhang and others, 2008a, 2010a, 2010b), but the model is not yet fully demonstrated. For instance, short duration (~1 Ma) is a key feature of plume head-generated LIPs (White and McKenzie, 1989; Griffiths and Campbell, 1990), but available data show a relatively long duration (~5 Ma) for the TLIP (Tian and others, 2010; Yu and others, 2011a; Zhang and others, 2012b). Previous investigations show that the ultramafic-mafic-felsic layered intrusions and felsic volcanic rocks were formed at 272 to 284 Ma (Yang and others, 1996, 2006b; Li and others, 2007; Zhang and others, 2008a, 2009b, 2010b; Tian and others, 2010; Wei and Xu, 2011; Yu and others, 2011a). However, currently available age data on basaltic lavas are highly variable, ranging from 260 to 293 Ma (Li and others, 2011; Qin and others, 2011 and references therein). Most of these earlier dates are based on K-Ar techniques, and await confirmation by robust $^{40}Ar/^{39}Ar$ dating or other methods. For example, recent LA-ICPMS zircon U-Pb dating revealed that the basalts in the northern Tarim Craton were formed at 286 to 291 Ma (Tian and others, 2010), significantly earlier than the intrusive events. Similar results have been obtained by U-Pb dating of zircons extracted from basalt flows in Keping (Yu and others, 2011b; Zhang and others, 2012b).

There is debate over the relative roles of lithospheric mantle and crust contributions to several flood basalt provinces such as the Paraná–Etendeka and the Karoo–Ferrar (for example, Hergt and others, 1991; Arndt and Christensen, 1992; Ellam and others, 1992; Gibson and others, 1995; Turner and others, 1996; Ewart and others, 1998; Peate and others, 1999; Rocha and others, 2012). A similar debate is still centering on the origins and petrogenesis of the TLIP (Jiang and others, 2004; Li and others, 2008, 2012a, 2012b; Zhou and others, 2009; Tian and others, 2010; Zhang and others, 2010b; Yu and others, 2011b).

With aims of resolving the afore-mentioned issues on the age of the Keping basalts and petrogenesis, we carried out a systematic investigation into a well exposed section of early Permian basaltic lavas in Keping and basaltic dikes in Bachu which crosscut both the Carboniferous-Permian sedimentary rocks and Xiaohaizi syenite complex (fig. 1). We present new $^{39}Ar/^{40}Ar$ data on the Keping basalts, together with a careful screening of previously published geochronological data to further constrain the age

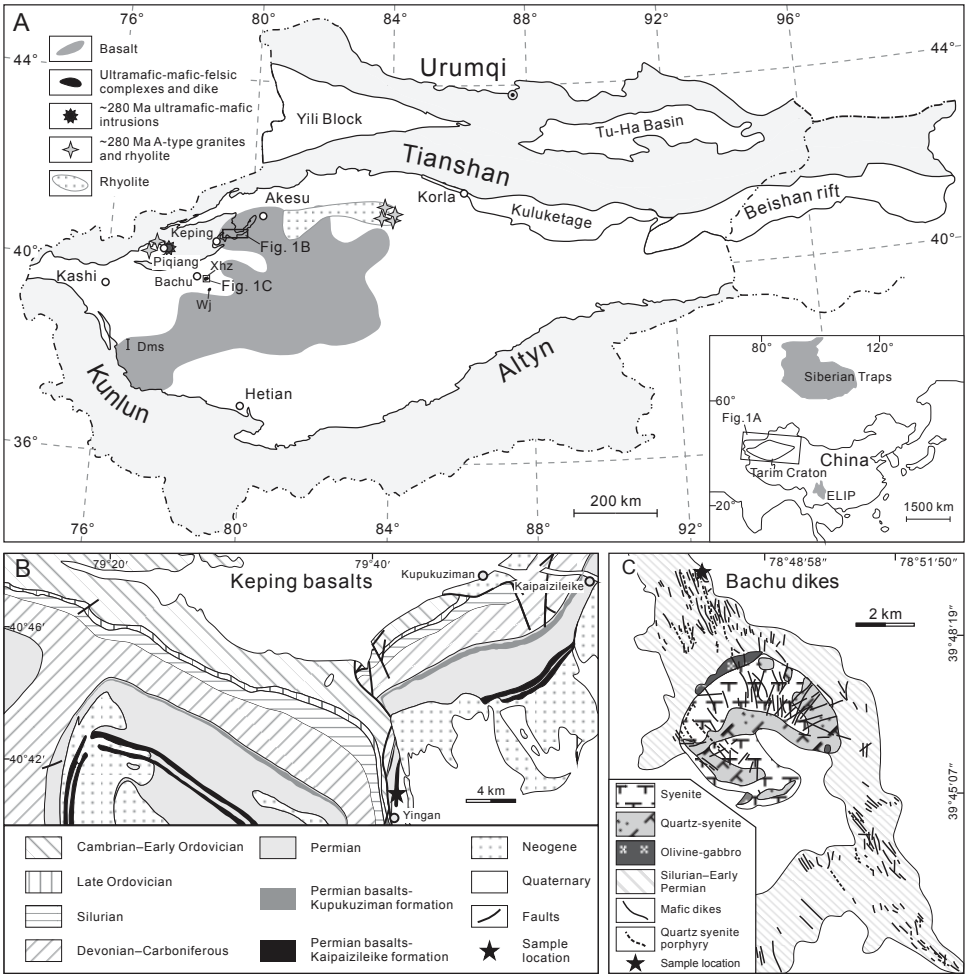

Fig. 1. (A) Simplified geological map of northwestern China, showing the distribution of the Permian basalts, ultramafic-mafic-felsic complexes, A-type granites and rhyolites in the Tarim Craton (modified after BGMRXUAR, 1993; XIGMR, 2007; Yang and others, 2007). Dms: Damusi section; Wj: Wajilitag area; Xhz: Xiaohaizi area. The lower right inset shows the locations of the Siberia Traps to the north and the ELIP to the south (modified after Zhou and others, 2009). (B) Sketch map of the Keping area showing outcrop and distribution of the Permian basalts (modified after the Wushi geological map of 1/200,000 scale; BGMRXUAR, 1993) and the sample location; (C) Detailed geological map of the mafic and felsic dikes around the Xiaohaizi syenite complex in Bachu (modified after Yang and others, 2007; Chen and others, 2010). Areas expanded in figures 1B and 1C are outlined on figure 1A.

of the basaltic lavas from the TLIP. With these dates and newly acquired major and trace element and Sr-Nd-Pb isotope data, we attempt (a) to investigate the genetic relationships of the Keping basalts and Bachu dikes, (b) to decipher the relative contributions of crust, lithospheric mantle and mantle plume, and (c) to understand the role of plume-lithosphere interaction in the temporal and spatial evolution of the TLIP.

GEOLOGICAL UNITS

The Tarim Craton, located in northwestern China, is bounded by Tianshan orogenic belt to the north and northwest, Beishan rift to the northeast, Kunlun

orogenic belt to the southwest and Altyn orogenic belt to the southeast (fig. 1A). The Tianshan orogenic belt is part of the Central Asian Orogenic Belt (CAOB) which is the largest Phanerozoic orogen in the world and has a complex evolutional history represented by multi-stage subduction and juvenile crustal growth (Han and others, 2011 and references therein). The Beishan rift, located in the northeastern part of the Tarim Craton, was developed during the Carboniferous and Permian (BGMRXUAR, 1993; Su and others, 2012). It is commonly believed that the Tarim Craton was amalgamated to the CAOB in the late Carboniferous indicated by the West Tianshan high to ultrahigh pressure metamorphic rocks including coesite-bearing eclogites (Lü and others, 2008; Han and others, 2011). The Tarim Craton is composed of a deformed and metamorphosed Precambrian basement consisting mainly of (1) Archean tonalite–trondhjemite–granodiorite (TTG) gneisses and amphibolites, (2) Palaeoproterozoic metamorphic mafic and felsic intrusions, schist and marble, (3) Mesoproterozoic to early Neoproterozoic low grade metamorphic rocks including metamorphosed carbonate, clastic rocks and granitoids and (4) middle to late Neoproterozoic mafic dikes, bimodal volcanic rocks, granitoids and glacial deposits, which crop out along the margins of the craton, for example, Kuluketage, Keping, Altyn and southwestern Tarim (BGMRXUAR, 1993; Hu and others, 2000; Xu and others, 2005, 2009; Zhang and others, 2007, 2012a; Lu and others, 2008; Long and others, 2010, 2011; Cao and others, 2011; Zhu and others, 2011). The basement is overlain by a thick sequence of Phanerozoic shallow marine and terrestrial sandstones, siltstones, shales, dark limestone, chert and volcanic rocks (BGMRXUAR, 1993; Cao and others, 2011). Several important phases of igneous activity have been identified in the Tarim Craton, including Neoarchaean, Palaeoproterozoic, Mesoproterozic, Neoproterozoic and early Permian events (BGMRXUAR, 1993; Hu and others, 2000; Long and others, 2010). Among these, the early Permian phase is the most extensive and considered to be a LIP probably related to mantle plume activity (Li and others, 2008; Pirajno and others, 2008; Zhang and others, 2008a, 2010b, 2010c; Zhou and others, 2009; Tian and others, 2010; Yu and others, 2011b).

Because the majority of the Permian igneous rocks are buried by a thick succession of post-Permian strata, and exposures around the craton margins are difficult to access, its full extent is not clear. However, industrial geophysical surveys showed that the Permian basalts may extend over an area of 250,000 km^2 in the Tarim Craton (Yang and others, 2007; Tian and others, 2010). Geophysical data indicate that the lava thickness exceeds 2500 m in the northern Tarim Craton (Tian and others, 2010). The early Permian basalts occur mainly in the northwestern and southwestern parts of the craton, with significant exposures in the Keping area (fig. 1A). In the Keping area, a complete early Permian basalt succession is exposed in the Yingan, Kupukuziman and Kaipaizileike areas (fig. 1B). Numerous dikes occur in the Bachu area.

Keping Basalts

The Permian basaltic sections, situated near the Yingan and Kupukuziman village, about 45 km northeast of Keping in the northwestern Tarim Craton, has been described in detail by Jiang and others (2004) and Yu and others (2011b). In this area, late Neoproterozoic to Permian sedimentary strata are well exposed and folded, providing a good opportunity to investigate the Paleozoic evolution of the Tarim Craton. The Permian basalt-dominated sequence is divided into the lower to middle Permian Kupukuziman Formation and the overlying middle Permian Kaipaizileike Formation (fig. 1B). The Kupukuziman Formation conformably overlies the upper Carboniferous–lower Permian sedimentary rocks. The lower part of Kupukuziman Formation mainly consists of graywacke and siltstone, and the upper part of two discrete basalt units with a total thickness of 10 to 75 m. The two basalt units are separated by several meters of terrestrial sedimentary rocks and overlain by a ~10 m

thick grayish-green tuff bed. The overlying Kaipaizileike Formation is subdivided into two subgroups. The lower subgroup is mainly composed of graywacke and siltstone with a total thickness of ~800 m and the upper one comprises six basaltic flows interlayered with fluvial sedimentary rocks with individual basaltic flows ranging from ~20 m to ~70 m thick and total thickness from ~100 to ~400 m. Sedimentary rocks in the Kupukuziman and Kaipaizileike Formations consist mainly of siltstones and silty lutites in the upper part, and graywackes and siltstones in the middle and lower parts. Abundant plant fossils (for example, *Lepidodendron sp., Stigmaria ficoides* Brongniart) have been reported in the graywackes, siltstones and silty lutites (Wu and others, 1997), indicating a terrestrial depositional environment the lavas were erupted into.

Bachu Dikes

The study region is located in the Xiaohaizi area, and is close to the Bachu city, in the northwestern part of the Tarim Craton. The strata in this area are largely covered by Quaternary sequences, with a few outcrops occurring around the Xiaohaizi reservoir composed of Silurian, Devonian, Carboniferous and lower Permian strata (fig. 1C). The early Permian Xiaohaizi syenite complex is composed of syenite and quartz syenite, and intrudes the Silurian-early Permian strata. Subordinate olivine-gabbro cumulates occur around the complex. The mafic dikes in the Xiaohaizi area cross-cut the sedimentary rocks with nearly vertical dips and variable strikes, but mainly northwest-trending. The dikes also intrude the Xiaohaizi syenite complex although some of the dikes intermingle with the syenite. At several outcrops bimodal dikes, consisting of diabase and quartz syenite porphyry, were observed.

PETROGRAPHY

Keping Basalts

The samples were collected from the Kaipaizileike Formation. They are fine-grained with variable amounts of plagioclase (1-5%) and clinopyroxene (5-10%) phenocrysts. Minor olivine phenocrysts (<1%, totally iddingsitized) occur in some samples. The groundmass contains plagioclase, clinopyroxene and oxides with minor olivine. A more detailed petrographic description of the basalts has been given by Yu and others (2010, 2011b).

Bachu Dikes

The Bachu mafic dikes have similar textures to the Keping basalts but contain only minor plagioclase phenocrysts (<1%). They are moderately altered with plagioclase partially changed to sericite and clinopyroxene to opaque minerals (for example, Fe-Ti oxide).

ANALYTICAL METHODS

Sample chips (~1 cm in size) obtained from the central parts of the samples were washed once with tap water, and then twice with 2 percent HCl followed by twice with Milli-Q water. They are hand-picked to avoid weathering rinds, amygdales, veins and areas of strong alteration. One split of picked chips was powdered in a tungsten carbide mill for major element analysis, while a second was further crushed to 0.6 to 1.0 mm size in a tungsten carbide percussion mill, washed twice with Milli-Q water in an ultrasonic bath for 20 minutes and then powered by hand in an agate mortar under a fume hood for trace element and isotope analysis.

Major element analyses were performed at the Guangzhou Institute of Geochemistry, Chinese Academy of Sciences (GIG-CAS). Trace element and Sr-Nd-Pb isotope analyses were carried out at the University of Queensland, Australia. Major element oxides were determined by standard X-ray fluorescence (XRF). Samples were pre-

pared as glass discs using a Rigaku desktop fusion machine. Analyses were performed on a Rigaku ZSX100e instrument at GIG-CAS following the procedure described by Li and others (2006). Analytical uncertainties are mostly between 1 percent and 5 percent.

Approximately 60 mg of each rock powder was dissolved in Savillex™ Teflon beakers with a distilled HF-HNO_3 (4:1) mixture. The dissolution was maintained on a hotplate at 110 °C for 7 days. The solutions were then dried down to evaporate HF. The sample residues were re-dissolved with double quartz-distilled concentrated HNO_3 followed by 1:1 HNO_3 and dried again. Finally, the samples were dissolved in a final 8 ml 5 percent HNO_3 stock solution. A weighed aliquot of this stock solution, corresponding to ~2 mg of the starting powder, was mixed with an internal standard containing ^{6}Li, ^{61}Ni, Rh, In, Re, Bi, and ^{235}U and diluted with 2 percent HNO_3 to achieve a final dilution factor of about 1:5000 for trace element analysis. The remaining stock solution was retained for Sr-Nd-Pb column chemistry. These analyses were performed at the Radiogenic Isotope Facility, School of Earth Science, the University of Queensland on a Thermo XSeriesII ICP-MS following the protocol of Eggins and others (1997) with modifications as described in Kamber and others (2003) and Li and others (2005). USGS standard W2 was used as a calibration standard and cross-checked with BIR-1. Instrumental drifts in mass reponse ware corrected with both the multi-element internal standard and an external drift monitor. Average full procedural blank values (mean of three separately prepared blanks from three runs, in pg, 1σ SD) for the key elements of this study are as follows: La (2.1 ± 1.0), Sm (0.8 ± 0.6), Nd (4.0 ± 2.3), Lu (0.1 ± 0.1), Nb (21.4 ± 3.1), Ta (16.2 ± 2.9), Th (0.7 ± 0.3), U (0.8 ± 0.4) and Pb (31.2 ± 1.5).

Isotope ratios of Sr, Nd and Pb were obtained on the remaining stock solution left from the trace element analyses. Sr, Nd and Pb chemical separations were performed following a modified procedure described by Pin and Zalduegui (1997), Deniel and Pin (2001) and Míková and Denková (2007). Strontium was separated from Rb and purified using Sr-Spec resin and deposited on Ta filaments with TaF_5. Sr isotope ratios were measured fully automatically on a 20-year-old VG Sector 54 thermal ionization mass spectrometer (TIMS) in a three-sequence dynamic mode using $^{86}Sr/^{88}Sr = 0.1194$ for exponential mass fractionation corrections. The NBS-987 standard was used as a monitor of the detector efficiency drift of the instrument. It was repeatedly measured during the analysis of the samples (n = 45) and yielded an average of 0.710222 ± 20 (2σ). The deviation of this mean value from the laboratory's previously obtained long-term average of 0.710249 ± 28 (2σ) was used to correct for all samples. Nd was separated using Ln-Spec resin (Pin and others, 1997). Nd isotopes were analyzed fully automatically on a Nu Plasma multi-collector inductively coupled plasma mass spectrometer (MC-ICPMS), using a three-sequence dynamic procedure. Instrumental bias and mass fractionation were corrected for by normalizing raw ratios to $^{146}Nd/^{144}Nd = 0.7219$. During the period of this study, the Ames Nd metal standard was used to estimate reproducibility (0.000016; 2σ, n = 17), and the $^{143}Nd/^{144}Nd$ data are presented relative to an Ames Nd metal $^{143}Nd/^{144}Nd$ value of 0.511966. Accuracy was assessed by analyzing the JNdi-1 Nd standard and the BHVO-2 USGS rock standard. The JNdi-1 standard yielded $^{143}Nd/^{144}Nd = 0.512113 \pm 9$ (2σ, n = 11), consistent with the expected value: 0.512115 ± 7 (Tanaka and others, 2000), and BHVO-2 yielded $^{143}Nd/^{144}Nd = 0.512982 \pm 6$ (2σ, n = 2), identical to the recommended value (GeoReM: http://georem.mpch-mainz.gwdg.de/). Purification and elution of Pb were performed following a modified HCl procedure using Sr-spec resin (Deniel and Pin, 2001; Míková and Denková, 2007). Lead separated by column chemistry was doped with 4 ppb thallium with a $^{205}Tl/^{203}Tl$ ratio of 0.23875 used for mass fractionation correction. Repeated analyses of NBS 981 yielded average ratios of

$^{208}Pb/^{204}Pb = 36.7046 \pm 140$, $^{207}Pb/^{204}Pb = 15.4938 \pm 38$, $^{206}Pb/^{204}Pb = 16.9361 \pm 47$ ($n = 38$, 2σ). Lead isotope data are given relative to NBS 981 values of $^{208}Pb/^{204}Pb = 36.7179$, $^{207}Pb/^{204}Pb = 15.4944$, $^{206}Pb/^{204}Pb = 16.9410$ as reported by Collerson and others (2002).

For $^{40}Ar/^{39}Ar$ dating, samples were obtained from the cores of basalt blocks. Groundmass fragments were carefully hand-picked under a binocular microscope from crushed rocks (40-60 mesh size fractions). The samples were cleaned with acetone followed by further cleaning with Milli-Q water in an ultrasonic bath for 15 min and then dried at 90 °C. Samples and monitor standard ZBH-2506 Biotite were wrapped in aluminum foil, sealed in a quartz ampoule and then irradiated for 54 h in the 49-2 reactor in Beijing. The *J*-values for the samples were determined using ZBH-2506 Biotite (132.5 Ma) as a flux monitor. To obtain *J*-values for unknown samples, the monitor ZBH-2506 was packed between every four samples in quartz tubes, each tube containing four packets of ZBH-2506. Based on the *J*-values and the positions of ZBH-2506 in the sample tube, a regression line was obtained for each sample tube, and then the *J*-values for the unknown samples were calculated by interpolation from the regression line. A *J*-value uncertainty of 0.15 percent (1σ) was considered in the reported ages. The $^{40}Ar/^{39}Ar$ dating was performed at GIG-CAS using a GV5400 mass spectrometer following analytical procedures described by Qiu and Wijbrans (2008). Argon gas was extracted from the sample by step-heating using a COHERENT-50W CO_2 continuing laser. The released gases were purified by two Zr/Al getter pumps operated for 5 to 8 min at room temperature and ~450 °C respectively. The background of the sample holder is lower than 2 mV pre-experiment and 4 to 6 mV during the experiment after a 5 min evacuation, and the signal of the sample is controlled within the range of 40 to 200 mV. The $^{40}Ar/^{39}Ar$ dating results were calculated and plotted using the ArArCALC software (Koppers, 2002).

RESULTS

$^{40}Ar/^{39}Ar$ Ages

Two basalts from the Kaipaizileike Formation in Yingan, Keping area were selected for dating. The $^{40}Ar/^{39}Ar$ age results at the 2σ level are given in table 1 and figure 2. In figure 2, both the age spectra (figs. 2A and 2C) and the $^{40}Ar/^{36}Ar$ and $^{39}Ar/^{36}Ar$ isochron diagrams (fig. 2B and D) are shown.

Sample YG-2 displays decreasing apparent ages versus temperature (except for the very first steps) which converge towards ~281 Ma at high temperatures (fig. 2A). This shape nevertheless allows us to calculate a plateau age of 287.3 ± 4.0 Ma corresponding to more than 96 percent of ^{39}Ar released. Such decreasing shape could suggest ^{39}Ar and ^{37}Ar recoil from K- and Ca-rich sites during irradiation (Duncan and others, 1997; Hofmann and others, 2000; Jones and others, 2001; Martin and others, 2011). This sample has initial $^{40}Ar/^{36}Ar$ values (440) (fig. 2B) far higher than atmosphere, suggesting excess argon problems. The total fusion age of sample YG-2 is 286.7 ± 2.7 Ma, consistent with the plateau age of 287.3 ± 4.0 Ma and isochron age of 288.2 ± 5.3 Ma.

Sample YG-14 yields a well-defined plateau age of 287.9 ± 3.1 Ma, which constitutes greater than 98 percent of the total ^{39}Ar released (fig. 2C). The correlation diagram ($^{40}Ar/^{36}Ar$ versus $^{39}Ar/^{36}Ar$; fig. 2D) displays an age of 287.4 ± 3.1 Ma consistent with the plateau age and total fusion age (287.6 ± 2.7 Ma), with initial $^{40}Ar/^{36}Ar$ ratio (290.9) approximate to atmospheric composition. This sample is thus unaffected by significant argon loss or excess argon based on the age spectra.

Major and Minor Elements

Major and trace element data for representative samples are given in table 2. In our dataset, the silica and alkali contents of the Keping basalts (except YG-21) range

TABLE 1

$^{40}Ar/^{39}Ar$ dating results of the Keping basalts

Incremental Heating		$^{36}Ar(a)$	$^{38}Ar(cl)$	$^{39}Ar(k)$	$^{40}Ar(r)$	Age ± 2σ	$^{40}Ar(r)$	$^{39}Ar(k)$
Steps	Laser (%)	(V)	(V)	(V)	(V)	(Ma)	(%)	(%)
(a) YG-2 (whole rock); J=0.00360								
10G2204D	5.0	0.026	0.010	9.132	455.610	298.1 ± 1.2	98.36	11.75
10G2204E	5.4	0.012	0.009	9.362	458.827	293.2 ± 1.2	99.23	12.05
10G2204G	5.8	0.005	0.007	8.231	398.553	290.0 ± 1.2	99.62	10.59
10G2204H	6.2	0.002	0.005	6.041	292.708	290.1 ± 1.3	99.80	7.77
10G2204I	6.8	0.001	0.006	5.812	279.134	287.8 ± 1.2	99.85	7.48
10G2204J	7.5	0.004	0.013	10.208	487.209	286.1 ± 1.2	99.77	13.13
10G2204L	8.0	0.005	0.008	6.644	315.596	284.9 ± 1.2	99.57	8.55
10G2204M	9.0	0.003	0.007	4.607	217.984	283.8 ± 1.2	99.61	5.93
10G2204N	10.5	0.003	0.007	5.456	254.749	280.4 ± 1.2	99.60	7.02
10G2204O	12.0	0.004	0.003	2.897	136.955	283.6 ± 1.3	99.20	3.73
10G2204Q	16.0	0.007	0.007	6.212	292.888	282.9 ± 1.2	99.33	7.99
10G2204R	19.0	0.002	0.001	0.654	30.948	284.1 ± 4.3	98.51	0.84
T1=287.3±4.0 Ma; T2=286.7±2.7 Ma; T3=288.3±5.3 Ma; T4=281.5±5.0 Ma								
(b) YG-14 (whole rock); J=0.00372								
10G2208D	4.8	0.040	0.002	1.811	82.712	283.0 ± 6.3	87.46	1.80
10G2208E	5.1	0.031	0.003	2.578	120.115	288.3 ± 4.4	92.88	2.57
10G2208G	5.5	0.024	0.004	6.572	309.229	290.9 ± 2.2	97.71	6.54
10G2208H	5.8	0.020	0.003	5.007	233.623	288.6 ± 1.3	97.51	4.99
10G2208I	6.3	0.014	0.008	9.291	443.546	294.8 ± 1.3	99.06	9.25
10G2208J	6.7	0.007	0.011	11.361	536.335	291.8 ± 1.2	99.63	11.31
10G2208L	7.2	0.003	0.009	8.144	379.489	288.3 ± 1.1	99.76	8.11
10G2208M	7.8	0.005	0.010	11.292	525.654	288.0 ± 1.1	99.72	11.25
10G2208N	8.3	0.003	0.006	7.009	324.912	286.9 ± 1.2	99.75	6.98
10G2208O	9.0	0.002	0.008	6.454	298.968	286.7 ± 1.2	99.82	6.43
10G2208Q	10.0	0.005	0.006	5.745	265.124	285.7 ± 1.2	99.46	5.72
10G2208R	12.0	0.004	0.005	4.511	208.036	285.5 ± 1.4	99.37	4.49
10G2208S	16.0	0.011	0.015	13.539	624.990	285.8 ± 1.1	99.47	13.48
10G2208T	20.0	0.008	0.005	4.168	191.069	283.9 ± 1.2	98.85	4.15
10G2208V	26.0	0.003	0.001	1.490	68.735	285.6 ± 2.9	98.91	1.48
T1=287.9±3.1 Ma; T2=287.6±2.7 Ma; T3=287.4±3.1 Ma; T4=287.8±3.5 Ma								

T1: Weighted plateau age; *T2*: total fusion age; *T3*: isochron age; *T4*: inverse isochron age. All ages are given at the 2σ.

from 44.4 to 48.3 weight percent (all normalized to 100%) and from 3.9 to 4.9 weight percent, respectively. The Bachu dikes have more variable silica (45.7-52.2 wt.%) and alkali (3.0-6.2 wt.%) contents than the Keping basalts. On the volatile-free total alkali-SiO_2 diagram (fig. 3A), the Keping basalts (except YG-21 which has anomaly high Na_2O contents of 6.35 wt.%) show a tight distribution, with an alkaline basaltic affinity. However, the Bachu dikes straddle the line separating alkaline and sub-alkaline basalts (fig. 3A), probably due to Na_2O and K_2O mobility during alteration, in accordance with their high LOI contents (1.8-4.2 wt.%). The Zr/TiO_2 versus Nb/Y diagram (Winchester and Floyd, 1977), therefore, is utilized for rock classification, because all the elements are generally considered to remain immobile during alteration/weathering. On the diagram (fig. 3B), the Keping basalts tightly cluster near the

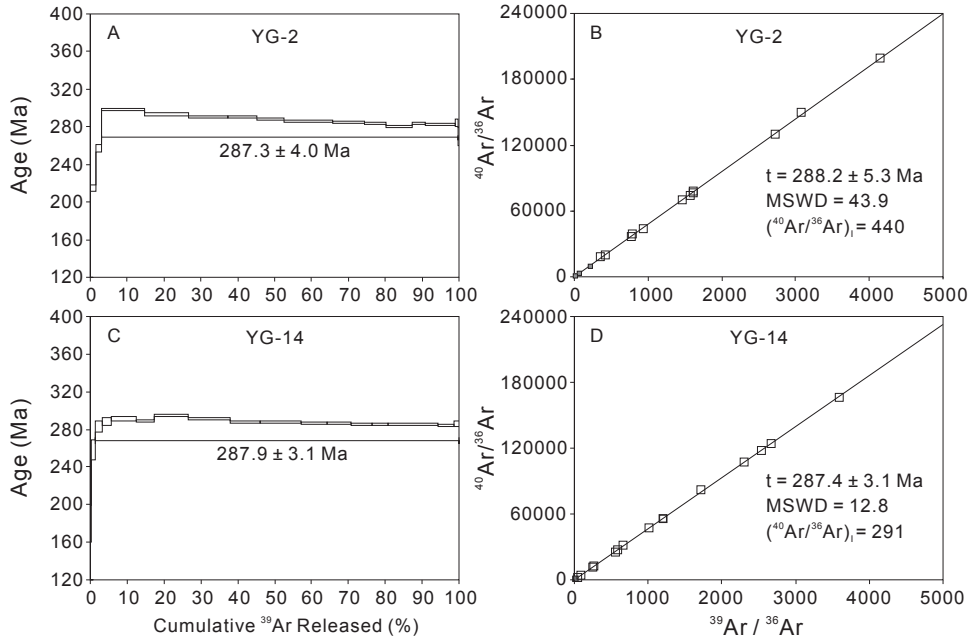

Fig. 2. $^{40}Ar/^{39}Ar$ plateau age spectra and $^{40}Ar/^{36}Ar$ versus $^{39}Ar/^{36}Ar$ correlation of the whole rocks for the Keping basalts. All ages are given at the 2σ level. On isochron plots, open squares are data used to determine isochrons.

alkaline-subalkaline boundary line, and the Bachu dikes fall in the field of alkaline basalts.

All the Keping basalts have TiO_2 contents of 3.09 to 5.1 weight percent and Ti/Y ratios of 548 to 964, comparable to the high-Ti basalts of the ~260 Ma Emeishan large igneous province (ELIP) in southwestern China (Xu and others, 2001). MgO of the Keping basalts varies between 4.3 and 5.9 weight percent and Fe_2O_3T ranges from 15.6 to 19.0 weight percent, corresponding to Mg# [atomic ratio of $100Mg/(Mg + Fe^{2+})$] between 42 and 32. The Bachu dikes have similar MgO (3.6-5.4 wt.%), relatively low Fe_2O_3T (11.9-17.2 wt.%) and similar Mg# (36-41). The Keping basalts have higher P_2O_5 (0.78-1.51 wt.%) contents than the Bachu dikes (0.40-0.69 wt.%). These rocks display very low concentrations of compatible elements Ni (3.1-77.8 ppm), Sc (17.2-28.8 ppm) and Co (30-53.2 ppm). The Keping basalts show higher Cr (47.3-78 ppm) contents than the Bachu dikes (0.08-39.7 ppm) and the majority of the Bachu dikes have extremely low Cr values of 0.08-0.69 ppm.

On the plots of major elements against MgO (fig. 4), the Keping basalts form compositional trends that are distinct from those defined by the Bachu dikes. Fe_2O_3T, TiO_2 and P_2O_5 in the Keping basalts increase and Al_2O_3 decreases with decreasing MgO. No correlation was observed between CaO and MgO. In contrast, with decreasing MgO the Bachu dikes show a systematic decrease in TiO_2, Fe_2O_3T and CaO, and an increase in Al_2O_3.

Trace Elements

The Keping basalts have very uniform chondrite-normalized rare earth element (REE) patterns (fig. 5A) with enrichment of light REE (LREE) over heavy REE (HREE) [$(La/Yb)_N = 6.3\text{-}7.7$] and very weak Eu anomalies ($Eu/Eu^* = 0.90\text{-}0.97$). On

TABLE 2

Major and trace elements for the Keping basalts and Bachu dikes

Sample	Keping basalts										
	YG-1	YG-2	YG-3	YG-5	YG-6	YG-7	YG-10	YG-11	YG-12	YG-13	YG-14
Major element (wt.%)											
SiO_2	46.27	46.57	44.93	46.68	46.16	45.41	47.87	47.18	46.74	46.80	46.44
TiO_2	4.14	4.21	4.14	4.02	4.16	3.93	3.83	3.81	3.73	3.71	3.72
Al_2O_3	13.16	13.19	13.52	13.59	13.10	14.52	13.60	13.56	13.63	13.70	13.84
Fe_2O_3T	16.78	17.11	16.84	16.46	17.36	16.09	15.62	15.34	15.57	15.28	15.38
MnO	0.21	0.21	0.20	0.19	0.22	0.18	0.19	0.18	0.19	0.18	0.16
MgO	4.21	4.57	5.27	4.81	4.85	4.98	4.67	5.12	5.39	5.59	5.48
CaO	7.86	7.79	7.47	7.79	7.80	8.13	8.53	8.39	8.40	8.40	8.39
Na_2O	3.28	3.10	3.08	3.32	2.74	2.63	2.51	2.46	2.48	2.40	2.65
K_2O	1.46	1.47	1.48	1.58	1.48	1.30	1.55	1.47	1.40	1.39	1.35
P_2O_5	1.30	1.28	1.15	1.10	1.30	0.96	0.82	0.82	0.77	0.78	0.77
LOI	0.86	0.02	1.42	0.00	0.86	1.40	0.35	1.20	1.22	1.31	1.35
Total	99.53	99.53	99.49	99.53	100.04	99.52	99.55	99.53	99.52	99.53	99.53
Mg#	33.2	34.6	38.3	36.7	35.6	38.0	37.2	39.8	40.7	42.0	41.4
Trace element (ppm)											
Sc	24.5	24.1	24.5	27.1	24.7	24.1	25.6	26.6	25.6	28.6	26.2
V	217	217	226	234	230	242	239	247	241	251	234
Cr	62.8	55.7	69.7	71.0	55.9	72.3	54.2	58.6	60.6	71.5	70.8
Co	46.6	47.0	48.6	51.4	47.8	53.2	46.4	46.5	47.1	45.7	47.6
Ni	54.6	55.8	64.1	60.0	56.4	77.8	45.5	48.7	54.1	54.1	61.5
Cu	50.6	50.2	48.8	50.1	51.0	45.6	42.7	43.3	42.4	46.4	48.6
Zn	174	172	168	174	182	164	160	165	155	151	153
Ga	22.5	22.2	22.0	23.5	22.8	22.4	22.2	21.9	21.7	21.9	22.1
Rb	19.0	13.9	23.7	30.4	21.1	21.8	29.0	28.2	26.8	26.0	24.0
Sr	341	359	307	361	360	353	331	315	307	319	309
Y	43.2	42.8	41.0	42.7	43.7	37.2	37.5	37.3	35.6	35.6	36.0
Zr	356	349	325	371	354	284	283	278	269	261	262
Nb	31.8	31.3	30.4	30.7	31.7	26.5	23.9	24.7	23.7	20.9	23.5
Cs	0.17	0.21	0.13	0.34	0.23	0.42	0.27	0.36	0.36	0.29	0.14
Ba	774	772	668	734	782	612	650	613	583	575	574
La	43.5	43.1	39.2	40.8	43.5	33.8	34.3	33.4	31.7	31.0	31.4
Ce	98.3	97.2	89.0	92.2	98.3	76.3	76.2	74.4	70.6	69.4	70.3
Pr	12.4	12.3	11.3	11.7	12.4	9.78	9.66	9.48	8.99	8.90	8.98
Nd	52.7	52.2	48.4	50.0	52.7	41.7	40.7	39.9	37.9	37.8	38.0
Sm	11.1	11.0	10.3	10.6	11.1	8.96	8.74	8.63	8.23	8.22	8.27
Eu	3.29	3.28	3.12	3.24	3.30	2.85	2.68	2.67	2.58	2.61	2.61
Gd	10.7	10.6	10.0	10.4	10.7	8.82	8.62	8.56	8.17	8.22	8.26
Tb	1.54	1.53	1.46	1.50	1.54	1.30	1.29	1.27	1.23	1.23	1.24
Dy	8.66	8.58	8.24	8.48	8.70	7.41	7.40	7.35	7.05	7.07	7.15
Ho	1.72	1.71	1.64	1.68	1.72	1.48	1.49	1.48	1.42	1.43	1.44
Er	4.56	4.50	4.33	4.48	4.57	3.95	4.01	3.98	3.82	3.81	3.85
Tm	0.62	0.62	0.59	0.62	0.63	0.55	0.56	0.56	0.54	0.53	0.54
Yb	3.86	3.80	3.69	3.83	3.90	3.39	3.52	3.50	3.39	3.34	3.39
Lu	0.57	0.57	0.55	0.57	0.58	0.50	0.52	0.52	0.50	0.50	0.50
Hf	7.63	7.53	6.99	7.61	7.70	6.21	6.34	6.26	6.10	5.91	5.93
Ta	1.76	1.76	1.73	1.71	1.74	1.50	1.28	1.40	1.31	0.98	1.36
Pb	6.97	6.90	5.72	6.56	7.06	5.37	6.48	6.21	5.69	5.53	5.77
Th	4.25	4.16	3.47	3.90	4.24	2.96	3.68	3.52	3.36	3.26	3.20
U	0.98	0.97	0.86	0.94	0.99	0.70	0.89	0.87	0.84	0.81	0.82

Mg# = $100Mg/(Mg + Fe^{2+})$; LOI: loss on ignition.

Table 2
(continued)

Sample	Keping basalts					Bachu dikes					
	YG-15	YG-19	YG-20	YG-21	YG-22	BC-0	BC-1	BC-2	BC-3	BC-4	BC-5
Major element (wt.%)											
SiO_2	46.14	43.88	44.01	43.74	45.02	49.84	46.77	45.70	49.02	44.09	44.90
TiO_2	3.73	4.93	5.06	3.97	3.89	2.95	3.42	3.77	3.34	3.94	4.58
Al_2O_3	13.58	12.95	12.64	13.72	14.26	14.82	14.61	14.36	14.53	13.23	14.08
Fe_2O_3T	15.79	18.48	18.68	15.83	16.36	11.82	12.74	15.11	13.43	16.62	15.36
MnO	0.20	0.22	0.23	0.18	0.18	0.15	0.15	0.17	0.16	0.16	0.19
MgO	5.76	4.68	4.48	4.97	5.40	3.51	4.41	4.39	3.85	5.18	4.88
CaO	8.40	7.50	7.53	7.46	8.01	6.85	7.20	8.77	7.89	9.60	7.69
Na_2O	2.59	2.60	2.49	6.26	3.43	3.18	3.19	3.21	2.65	2.29	3.42
K_2O	1.36	1.67	1.75	1.42	1.33	1.82	2.25	1.22	2.20	0.95	1.26
P_2O_5	0.80	1.44	1.49	1.05	0.93	0.54	0.66	0.45	0.46	0.38	0.54
LOI	1.69	1.12	1.11	0.91	0.71	4.22	4.23	2.43	2.06	3.12	2.62
Total	100.05	99.47	99.47	99.52	99.52	99.71	99.65	99.58	99.58	99.55	99.53
Mg#	41.9	33.4	32.2	38.3	39.5	37.0	40.7	36.5	36.2	38.2	38.6
Trace element (ppm)											
Sc	25.0	26.5	28.8	23.5	23.0	18.6		23.9	21.5	26.2	17.9
V	224	243	250	211	212	160		305	242	370	254
Cr	69.0	55.5	47.3	78.0	71.6	0.27		0.56	0.22	0.59	0.48
Co	48.0	48.6	49.3	50.6	51.0	35.0		46.0	36.5	55.0	41.3
Ni	61.8	40.8	39.1	71.0	71.8	8.75		22.9	18.5	45.6	4.69
Cu	49.8	50.2	52.2	48.3	45.4	39.3		125	72.0	169	22.0
Zn	159	196	208	167	161	128		135	135	139	168
Ga	22.3	24.0	24.3	22.3	22.4	22.9		24.0	23.3	23.6	23.9
Rb	27.2	31.8	31.9	25.1	24.5	46.9		29.3	43.9	18.1	21.9
Sr	309	289	296	347	336	576		592	681	494	581
Y	37.0	49.7	51.3	38.9	36.3	31.1		27.3	28.0	24.4	29.1
Zr	274	400	410	315	294	305		255	275	218	299
Nb	23.9	37.5	39.4	29.7	26.7	45.3		48.1	41.9	37.3	57.3
Cs	0.21	0.19	0.21	0.14	0.30	0.62		0.11	0.26	0.29	0.08
Ba	603	782	826	672	626	669		515	655	346	442
La	32.3	48.6	49.3	37.7	33.6	46.2		35.1	38.5	28.2	43.5
Ce	72.2	111	113	85.1	75.8	99.1		77.0	83.3	62.2	95.1
Pr	9.20	14.0	14.3	10.8	9.67	11.9		9.51	10.1	7.82	11.7
Nd	38.8	59.5	60.8	45.7	40.9	47.5		39.1	41.0	32.7	47.3
Sm	8.44	12.6	12.9	9.68	8.73	9.74		8.45	8.65	7.32	9.81
Eu	2.64	3.71	3.81	3.00	2.79	2.89		2.78	2.79	2.47	3.17
Gd	8.44	12.2	12.6	9.48	8.65	8.85		7.91	7.86	7.04	8.78
Tb	1.27	1.78	1.83	1.38	1.28	1.27		1.15	1.14	1.03	1.24
Dy	7.30	9.95	10.3	7.84	7.26	6.78		6.10	6.12	5.48	6.56
Ho	1.47	1.97	2.03	1.56	1.45	1.26		1.12	1.14	1.00	1.19
Er	3.95	5.24	5.40	4.13	3.87	3.19		2.80	2.90	2.48	2.94
Tm	0.56	0.72	0.74	0.57	0.54	0.41		0.35	0.37	0.31	0.36
Yb	3.50	4.43	4.55	3.53	3.36	2.47		2.08	2.23	1.84	2.16
Lu	0.52	0.66	0.68	0.53	0.50	0.35		0.29	0.31	0.25	0.29
Hf	6.16	8.51	8.76	6.77	6.40	7.13		6.17	6.54	5.35	6.89
Ta	1.32	2.08	2.21	1.68	1.49	2.69		2.83	2.50	2.25	3.42
Pb	5.52	6.74	7.15	5.53	5.22	5.04		3.81	4.39	3.81	3.80
Th	3.34	4.27	4.31	3.35	3.11	5.59		4.02	4.93	3.18	4.79
U	0.86	1.08	1.09	0.84	0.79	1.34		1.10	1.20	0.88	1.30

Mg# = $100Mg/(Mg + Fe^{2+})$; LOI: loss on ignition.

TABLE 2
(continued)

Sample	Bachu dikes			Standards					
	BC-6	BC-9	BC-12	BHVO-2	Ref.	BCR-2	Ref.	AGV-1	Ref.
Major element (wt.%)									
SiO_2	45.74	49.30	49.48	49.64	49.90			58.97	58.84
TiO_2	3.96	3.40	3.15	2.73	2.73			1.04	1.05
Al_2O_3	12.95	14.28	15.95	13.28	13.50			16.96	17.15
Fe_2O_3T	15.99	13.15	11.68	12.35	12.30			6.64	6.77
MnO	0.17	0.16	0.15	0.17	0.17			0.10	0.097
MgO	5.14	3.84	3.54	7.30	7.23			1.50	1.53
CaO	9.46	8.24	7.25	11.35	11.40			4.79	4.94
Na_2O	1.91	2.38	3.71	2.32	2.22			4.16	4.26
K_2O	0.99	1.88	2.37	0.51	0.52			2.86	2.92
P_2O_5	0.41	0.53	0.55	0.27	0.27			0.48	0.50
LOI	2.84	2.43	1.78						
Total	99.56	99.58	99.60						
Mg#	38.9	36.6	37.5						
Trace element (ppm)				n=12		n=5		n=2	
Sc	26.4	20.9	21.6	31.9	32.0	33.3	33.0	12.1	2.3
V	281	248	178	310	317	431	416	114	19
Cr	39.7	0.56	0.08	300	280	15.5	18.0	8.56	9.40
Co	46.7	47.0	30.0	45.0	45.0	37.5	37.0	15.2	15.2
Ni	57.4	21.6	3.09	117	119	11.8	18.0	14.5	15.5
Cu	110	96.5	22.2	130	127	22.3	21.0	56.9	58.0
Zn	130	145	129	115	103	131	127	87.6	87.0
Ga	21.6	25.2	24.2	21.2	22.0	21.7	23.0	20.6	20.2
Rb	21.6	44.8	50.1	9.17	9.11	47.0	46.9	67.3	66.6
Sr	504	699	760	398	396	338	340	665	660
Y	26.4	32.8	32.5	24.4	26.0	33.6	37.0	18.0	19.0
Zr	233	318	298	171	172	187	184	230	231
Nb	36.9	45.5	46.0	18.1	18.1	12.2	12.6	13.9	14.6
Cs	0.90	0.94	0.31	0.10	0.10	1.15	1.10	1.28	1.26
Ba	304	722	615	130	131	686	677	1305	1200
La	30.5	47.3	44.4	15.2	15.2	25.0	24.9	38.7	38.2
Ce	67.5	99.2	96.5	37.7	37.5	53.4	52.9	70.2	67.6
Pr	8.49	12.4	11.8	5.37	5.35	6.86	6.70	8.55	8.30
Nd	35.3	50.5	48.0	24.4	24.5	28.5	28.7	31.9	31.7
Sm	7.83	9.95	10.0	6.05	6.07	6.53	6.58	5.77	5.72
Eu	2.65	3.11	3.29	2.05	2.07	1.94	1.96	1.60	1.58
Gd	7.42	9.31	9.26	6.22	6.24	6.74	6.75	4.79	4.70
Tb	1.08	1.28	1.32	0.94	0.92	1.06	1.07	0.66	0.69
Dy	5.87	6.41	7.13	5.26	5.31	6.37	6.41	3.58	3.55
Ho	1.09	1.14	1.33	1.00	0.98	1.32	1.28	0.69	0.68
Er	2.73	2.86	3.36	2.51	2.54	3.64	3.66	1.86	1.82
Tm	0.34	0.38	0.43	0.33	0.33	0.53	0.54	0.26	0.28
Yb	2.05	2.29	2.61	1.97	2.00	3.37	3.38	1.64	1.63
Lu	0.28	0.33	0.37	0.27	0.27	0.50	0.50	0.25	0.24
Hf	5.68	8.20	7.03	4.34	4.36	4.83	4.90	5.09	5.10
Ta	2.22	3.03	2.72	1.11	1.14	0.74	0.74	0.80	0.87
Pb	3.55	6.08	4.23	1.57	1.60	9.92	11.0	33.6	37.4
Th	3.54	6.30	4.57	1.18	1.22	5.78	5.70	6.16	6.40
U	0.94	1.36	1.20	0.42	0.40	1.70	1.69	1.94	1.93

Mg# = $100Mg/(Mg + Fe^{2+})$; LOI: loss on ignition; Ref.: recommended values from http://georem.mpch-mainz.gwdg.de.

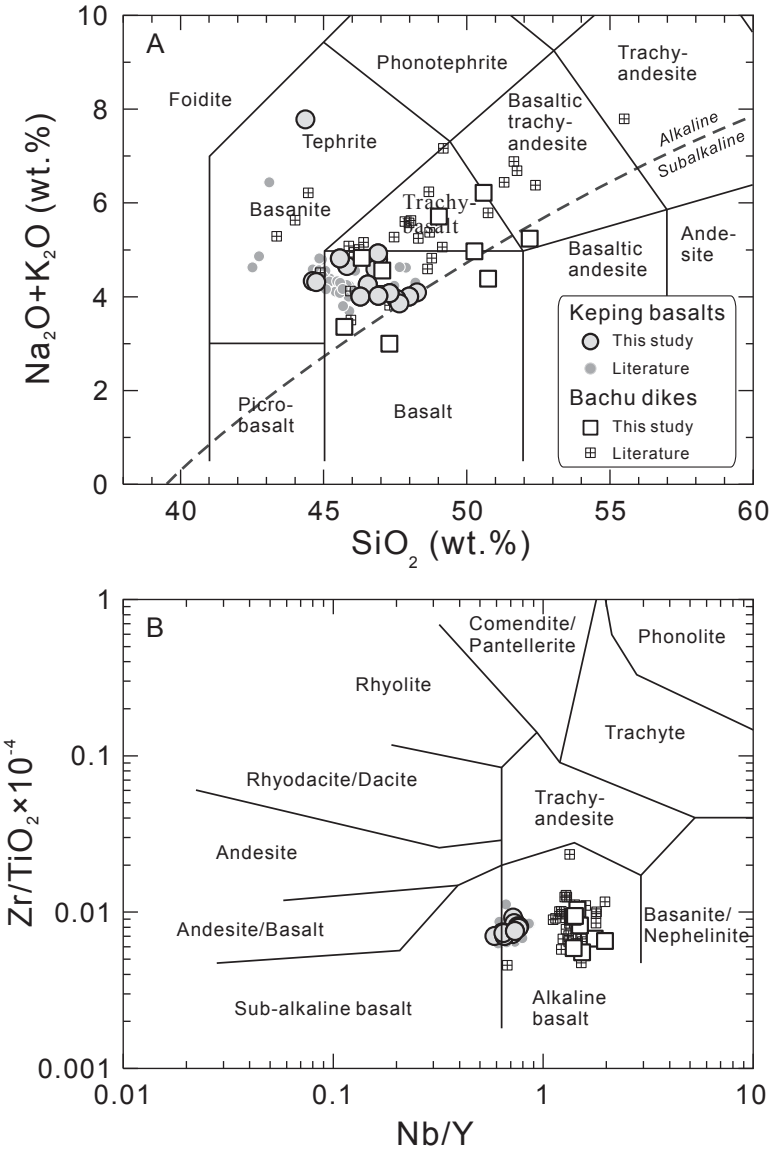

Fig. 3. (A) Total alkalis ($Na_2O + K_2O$) versus SiO_2 (TAS; Le Bas and others, 1986). The alkaline–subalkaline divide is from Irvine and Baragar (1971). (B) Zr/TiO_2 versus Nb/Y (Winchester and Floyd, 1977). Literature data sources: Keping basalts from Zhou and others (2009), Zhang and others (2010b), Yu and others (2011b) and Li and others (2012a); Bachu dikes from Zhou and others (2009) and Zhang and others (2010b). Five samples from Zhou and others (2009), three samples from Zhang and others (2010b) and one sample from Li and others (2012a) are excluded due to either significantly low or high Al_2O_3 contents at low MgO, highly incompatible with other samples within their dataset. This could be ascribed to abundant plagioclase phenocrysts (50 modal%; Zhou and others, 2009) in the samples.

primitive mantle-normalized multi-element diagrams, they show moderate enrichment in large ion lithophile elements (LILE) (Ba, Th, U) with pronounced Ba anomalies (fig. 5B). All the Keping basalts exhibit negative Nb, Ta and Sr anomalies, weak depletion in Pb, and marked positive P anomalies.

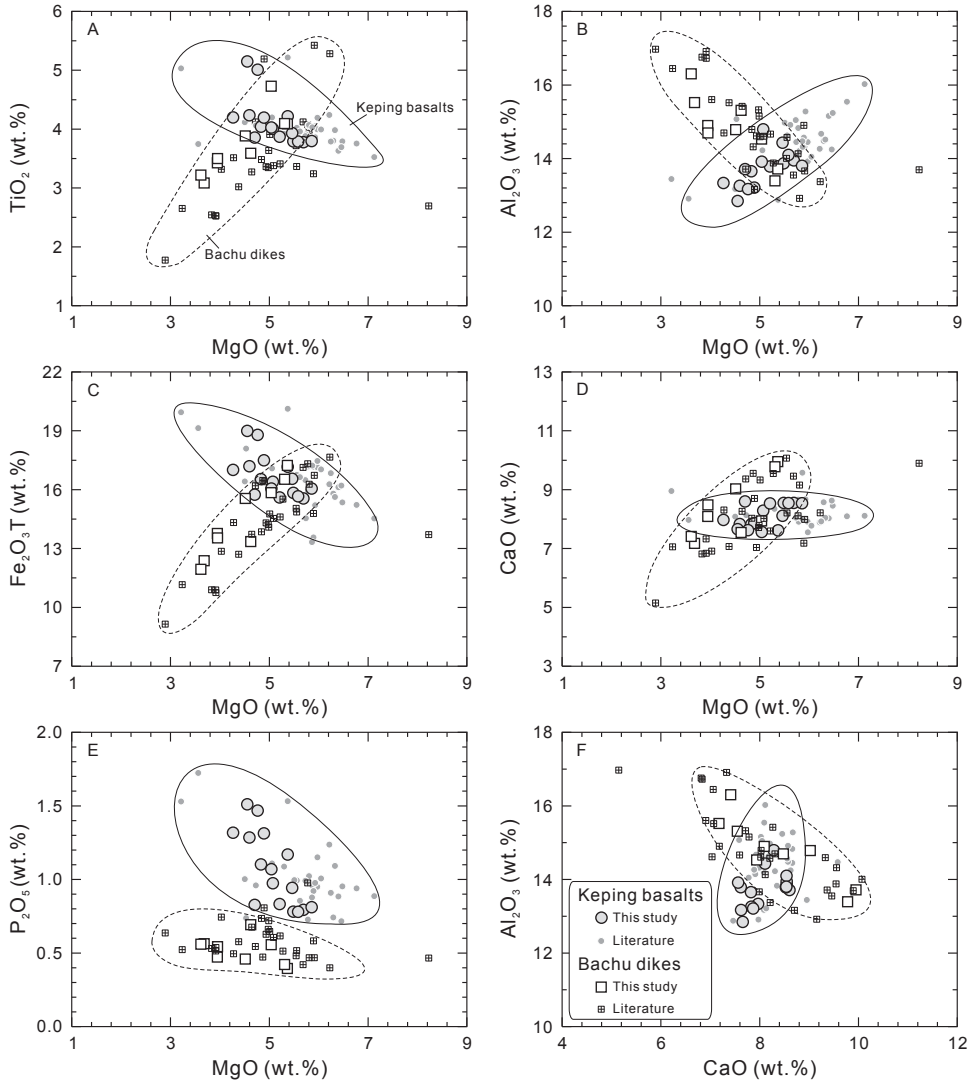

Fig. 4. Variation diagrams of selected major oxides against MgO and CaO. Solid and dashed outlined fields highlight the distinct evolutionary trends displayed by the Keping basalts and Bachu dikes, respectively. Literature data for the Keping basalts and Bachu dikes are shown for comparison. Literature data sources same as in figure 3.

The Bachu dikes display a more fractionated REE pattern than the Keping basalts on the chondrite-normalized REE plot (fig. 5C) with $(La/Yb)_N$ up to 19.7. They show slightly negative to positive Eu anomalies (Eu/Eu* = 0.93-1.04), pronounced peaks at Nb-Ta and troughs for Pb, similar to those of oceanic island basalts (fig. 5D) (OIB; Sun and McDonough, 1989). All the Bachu dikes are enriched in LILE, LREE, high field strength elements (HFSE) including Nb, Ta, Zr and Hf. Unlike the Keping basalts, only weak Sr and P anomalies are present in the Bachu dikes. Rb and Ba are more variable in some samples.

As illustrated in figure 5, the compositions of the samples analyzed in this study encompass those defined by published data for the Keping basalts and Bachu dikes

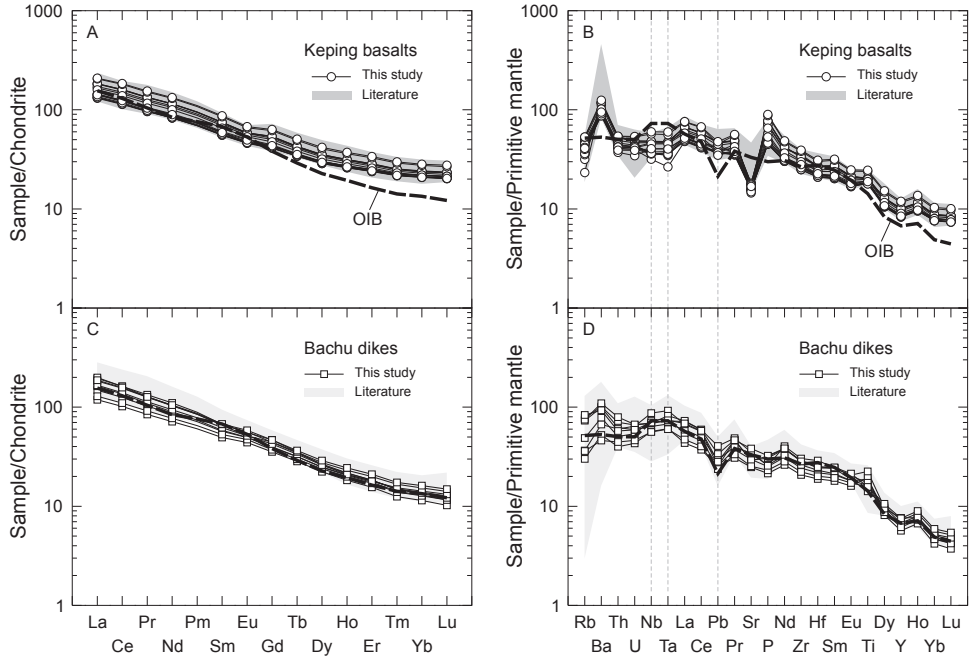

Fig. 5. Chondrite-normalized REE diagrams (A, C) and primitive mantle-normalized multi-element variation diagrams (B, D) for the Keping basalts and Bachu dikes. Shaded fields outline the compositional ranges defined by literature data of the Keping basalts and Bachu dikes, respectively. Also shown is a typical ocean island basalt (OIB) (dashed line) from Sun and McDonough (1989). Normalizing values from McDonough and Sun (1995). Literature data sources same as in figure 3.

(gray field; Zhou and others, 2009; Zhang and others, 2010b; Yu and others, 2011b; Li and others, 2012a).

Ratios of elements that are moderately to highly incompatible, for example, Zr/Nb and Ba/Th, are higher in the Keping basalts than in the Bachu dikes. In general, abundances of Y, Nb, Lu and U in these two groups are well correlated with Zr (figs. 6B, 6C, 6E and 6F). However, significant differences are noted between the two groups (fig. 6). For example, at a given Zr, the Bachu dikes have systematically higher Nb and U, and lower Y and Lu contents compared to the Keping basalts, indicating that they cannot have formed by fractional crystallization from a common parental magma.

Sr-Nd-Pb Isotopes

Sr-Nd-Pb isotope compositions are reported in table 3 and illustrated in figure 7. Isotopic ratios were back-calculated to their initial values at 290 Ma for the Keping basalts and at 280 Ma for the Bachu dikes (see discussion section for justification for choice of ages), respectively. The samples show relatively large variations in $(^{87}Sr/^{86}Sr)_i$, $(^{143}Nd/^{144}Nd)_i$, $(^{206}Pb/^{204}Pb)_i$, $(^{207}Pb/^{204}Pb)_i$ and $(^{208}Pb/^{204}Pb)_i$ (table 3), thus readily allowing discrimination of the two groups. The isotopic compositions obtained in this study are in good agreement with those previously published by Zhang and others (2010b), Yu and others (2011b) and Li and others (2012a), but are distinct from those of Zhou and others (2009).

The Keping basalts show a large range of $(^{87}Sr/^{86}Sr)_i$ (0.706166-0.707458) but a restricted range of $\varepsilon_{Nd}(t)$ (−3.9 to −2.4). On the plot of $\varepsilon_{Nd}(t)$ versus $(^{87}Sr/^{86}Sr)_i$ (fig.

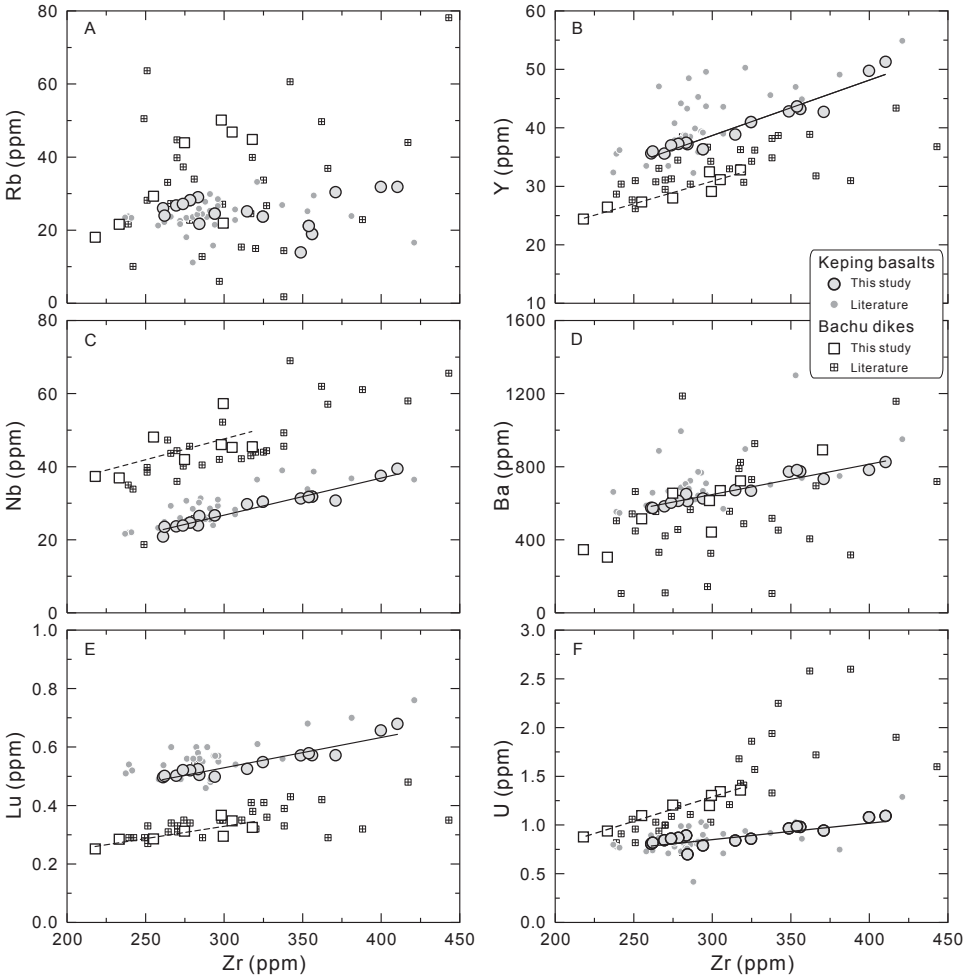

Fig. 6. Bivariate trace element plots to determine the extent of correlation of various immobile and mobile trace elements for both the Keping basalts and Bachu dikes. Solid and dashed lines represent regression lines for the Keping basalts and Bachu dikes in our dataset, respectively. Literature data sources same as in figure 3.

7A), they are displaced from the mantle array and lie in the enriched quadrant. Lead isotope ratio variability is relatively small, with relatively unradiogenic $(^{206}Pb/^{204}Pb)_i$ (17.427-17.566), radiogenic $(^{207}Pb/^{204}Pb)_i$ (15.508-15.530) and moderately radiogenic $(^{208}Pb/^{204}Pb)_i$ (37.925-38.016). In the Pb-Pb isotope space (figs. 7C and 7D), $(^{207}Pb/^{204}Pb)_i$ and $(^{208}Pb/^{204}Pb)_i$ positively correlate with $(^{206}Pb/^{204}Pb)_i$ and plot well above the Northern Hemisphere Reference Line (NHRL; Hart, 1984). A positive correlation is observed in the plot of $(^{143}Nd/^{144}Nd)_i$ versus $(^{206}Pb/^{204}Pb)_i$ (fig. 7B).

Compared with the Keping basalts, the Bachu dikes have higher $\varepsilon_{Nd}(t)$ varying from −0.3 to 4.6, and display larger variations in $(^{87}Sr/^{86}Sr)_i$ (0.705272-0.707625). The samples (except for BC-0, BC-3 and BC-9, which have lower Pb isotope ratios due to crustal contamination, discussed below) display more radiogenic $(^{206}Pb/^{204}Pb)_i$ (17.774-18.148), $(^{207}Pb/^{204}Pb)_i$ (15.557-15.590) and $(^{208}Pb/^{204}Pb)_i$ (38.184-38.410) than the Keping basalts, and plot close to the field defined by the least contaminated high-Ti

Table 3

Sr-Nd-Pb isotopes for the Keping basalts and Bahcu dikes

Sample	$\frac{^{87}Rb}{^{86}Sr}$	$\frac{^{87}Sr}{^{86}Sr}(2\sigma)$	$\left(\frac{^{87}Sr}{^{86}Sr}\right)_i$	$\frac{^{147}Sm}{^{144}Nd}$	$\frac{^{143}Nd}{^{144}Nd}(2\sigma)$	$\left(\frac{^{143}Nd}{^{144}Nd}\right)_i$	$\varepsilon_{Nd}(t)$	$\frac{^{206}Pb}{^{204}Pb}(2\sigma)$	$\frac{^{207}Pb}{^{204}Pb}(2\sigma)$	$\frac{^{208}Pb}{^{204}Pb}(2\sigma)$	μ	k	$\left(\frac{^{206}Pb}{^{204}Pb}\right)_i$	$\left(\frac{^{207}Pb}{^{204}Pb}\right)_i$	$\left(\frac{^{208}Pb}{^{204}Pb}\right)_i$
Keping basalts															
YG-1	0.1607	0.707971±7	0.707308	0.1269	0.512313±7	0.512072	-3.76	17.8396±13	15.5301±13	38.5155±40	8.86	39.67	17.432	15.509	37.939
YG-2	0.1124	0.707811±8	0.707347	0.1270	0.512310±10	0.512069	-3.82	17.8414±14	15.5302±13	38.5129±38	8.81	39.21	17.436	15.509	37.943
YG-3	0.2235	0.707408±8	0.706486	0.1282	0.512370±6	0.512127	-2.68	17.9407±15	15.5375±14	38.5326±43	9.49	39.53	17.504	15.515	37.958
YG-5	0.2441	0.708133±7	0.707126	0.1282	0.512325±7	0.512082	-3.57	17.8782±15	15.5345±14	38.5265±39	9.06	38.72	17.461	15.513	37.964
YG-6	0.1701	0.708035±7	0.707333	0.1272	0.512312±7	0.512071	-3.78	17.8413±12	15.5307±11	38.5178±41	8.80	39.09	17.436	15.510	37.950
YG-7	0.1781	0.706966±8	0.706231	0.1299	0.512394±5	0.512147	-2.29	17.9095±18	15.5362±18	38.4855±58	8.22	35.87	17.531	15.517	37.964
YG-10	0.2535	0.708168±10	0.707123	0.1296	0.512324±6	0.512078	-3.64	17.9229±13	15.5414±13	38.5200±37	8.70	36.96	17.523	15.521	37.983
YG-11	0.2589	0.708167±7	0.707098	0.1308	0.512339±6	0.512091	-3.40	17.9357±15	15.5421±14	38.5198±42	8.83	36.91	17.530	15.521	37.983
YG-12	0.2525	0.708072±13	0.707033	0.1313	0.512346±6	0.512096	-3.28	17.9626±13	15.5466±12	38.5495±30	9.37	38.59	17.531	15.524	37.989
YG-13	0.2358	0.708437±9	0.707464	0.1316	0.512345±5	0.512095	-3.31	17.9426±18	15.5423±17	38.5271±44	9.20	38.38	17.519	15.520	37.969
YG-14	0.2247	0.707697±8	0.706770	0.1317	0.512364±6	0.512114	-2.95	17.9489±12	15.5505±13	38.5562±43	8.96	36.20	17.537	15.529	38.030
YG-15	0.2541	0.707758±8	0.706710	0.1316	0.512378±6	0.512128	-2.66	18.0245±14	15.5539±14	38.5844±44	9.86	39.56	17.571	15.530	38.010
YG-19	0.3189	0.707571±10	0.706255	0.1280	0.512368±6	0.512125	-2.72	17.9639±12	15.5408±14	38.5602±40	10.11	41.32	17.499	15.517	37.960
YG-20	0.3115	0.707637±7	0.706351	0.1283	0.512365±6	0.512122	-2.79	17.9474±14	15.5395±13	38.5359±40	9.65	39.34	17.504	15.516	37.964
YG-21	0.2097	0.707428±8	0.706563	0.1280	0.512366±5	0.512123	-2.77	17.9333±15	15.5368±18	38.5256±46	9.58	39.52	17.492	15.514	37.951
YG-22	0.2117	0.707300±8	0.706426	0.1291	0.512375±5	0.512130	-2.63	17.9475±13	15.5379±12	38.5274±31	9.56	38.88	17.508	15.515	37.962
Bachu dikes															
BC-0	0.2352	0.706608±7	0.705671	0.1240	0.512504±5	0.512276	-0.02								
BC-2				0.1307	0.512758±6	0.512518	4.70	18.9408±15	15.6336±12	39.4145±38	18.64	70.63	18.113	15.591	38.424
BC-3	0.1866	0.707579±7	0.706836	0.1276	0.512541±6	0.512307	0.59	18.3017±16	15.5218±19	38.9321±54	17.47	73.96	17.526	15.482	37.895
BC-4	0.1059	0.706098±7	0.705676	0.1354	0.512757±5	0.512509	4.51	18.5078±14	15.5937±16	39.0398±43	14.76	55.28	17.853	15.560	38.264
BC-5	0.1091	0.706776±8	0.706341	0.1255	0.512735±8	0.512505	4.44	18.7622±20	15.6090±19	39.3785±48	22.15	84.17	17.779	15.558	38.198
BC-6	0.1241	0.705215±7	0.70472	0.1339	0.512731±6	0.512486	4.07	18.7059±12	15.5999±12	39.1615±40	16.99	66.27	17.952	15.561	38.232
BC-9	0.1856	0.706498±13	0.705758	0.1192	0.512481±7	0.512263	-0.29	18.1311±15	15.5352±16	38.7143±50	14.16	67.91	17.500	15.502	37.758
BC-12	0.1907	0.705487±7	0.704727	0.1263	0.512561±6	0.512330	1.02								

basalts from the ELIP (Zhang and others, 2006; Xu and others, 2007) (figs. 7C and 7D). In general, $(^{143}Nd/^{144}Nd)_i$, $(^{207}Pb/^{204}Pb)_i$ and $(^{208}Pb/^{204}Pb)_i$ positively correlate with $(^{206}Pb/^{204}Pb)_i$ (figs. 7B, 7C and 7D).

DISCUSSION

Age of the Keping Basalts and Bachu Dikes

Keping basalts.—Continental flood basalts older than a few million years have been inevitably affected by weathering/alteration, which may strongly affect the $^{40}Ar/^{39}Ar$ dating on whole-rock materials. However, the whole rock $^{40}Ar/^{39}Ar$ plateau ages defined by the less disturbed samples are in good agreement with corresponding plagioclase plateau ages (Renne and Basu, 1991; Duncan and others, 1997; Courtillot and others, 2000; Jones and others, 2001). Thus the plateau ages obtained in this study may represent crystallization ages of the Kaipaizileike Formation basalts. The relatively large 2σ errors (3-4 Ma) associated with the plateau ages could be ascribed to low temperature alteration (see LOIs in table 2; and also Baksi, 2007). Jourdan and others (2007b) suggest that the whole-rock $^{40}Ar/^{39}Ar$ ages are unreliable for high-precision (that is, less than a few hundred thousand years) geochronology applied to resolve the duration of the main magmatic pulse within a large igneous province. However, as the age data reported in this study are basically intended to provide constraint on the eruption age of the Keping basalts, the precision levels are thought to be robust. The $^{40}Ar/^{39}Ar$ plateau ages (287.3 ± 4.0 Ma and 287.9 ± 3.1 Ma, 2σ) of the Kaipaizileike Formation basalts obtained in this study are consistent with the SHRIMP U-Pb age (288.9 ± 2.0 Ma, 2σ; Yu and others, 2011b) of the basalt from the uppermost Kaipaizileike Formation within error.

Most of the previous published dates on the TLIP were obtained using a conventional K-Ar method and vary considerably from 260 Ma to 293 Ma (Li and others, 2011; Qin and others, 2011 and references therein). Alteration processes are probably the main cause of problems in the K-Ar age measurements (Sebai and others, 1991), resulting in the K-Ar ages being apparently too young, and older apparent ages could also occur if excess Ar is present in the sample, which cannot be identified from a single K-Ar age (Kaneoka, 1980). Due to the disturbed Ar isotopic systematics of the whole-rock samples, the K-Ar dating can only occasionally yield correct ages (Baksi, 1994; Baker and others, 1996). In addition, Yamasaki and others (2011) showed that the ages for the young basalts (<3 Ma) with altered groundmass olivine showing oxidation evidence are disturbed beyond the errors, probably because of K and/or Ar loss. Thus we will not utilize the K-Ar dates to constrain the age of the Keping basalts.

Yang and others (2006a) obtained whole-rock $^{40}Ar/^{39}Ar$ ages of 281.8 ± 4.2 Ma (2σ) and 290.1 ± 3.5 Ma (2σ) for the Kupukuziman Formation in Keping and Damusi, western Tarim Craton, respectively. However, the two samples have age spectra that display a general distinct decrease in apparent ages from low- to high-temperature steps, characteristic of whole rocks affected by strong ^{39}Ar recoil during irradiation and loss of ^{39}Ar (Baker and others, 1996; Duncan and others, 1997; Hofmann and others, 2000). Thus these results do not provide useful age constraints. Chen and others (1997a, 1997b) and Zhang and others (2010c) obtained $^{40}Ar/^{39}Ar$ plateau ages of 278.5 ± 1.4 Ma (2σ) and 282.9 ± 1.6 Ma (2σ) for the Kupukuziman Formation basalts which are significantly younger than zircon ages of 289.5 to 291.9 Ma (Yu and others, 2011b; Zhang and others, 2012b), and those from the northern Tarim Craton (286.6-290.9 Ma; Tian and others, 2010; Shangguan and others, 2011). In addition, these dates are inconsistent with the stratigraphic observation that the Kupukuziman Formation should be older than the overlying Kaipaizileike Formation (287-290 Ma; Yu and others, 2011b and this study). Therefore, the younger $^{40}Ar/^{39}Ar$ ages may not represent the crystallization age of the basalts.

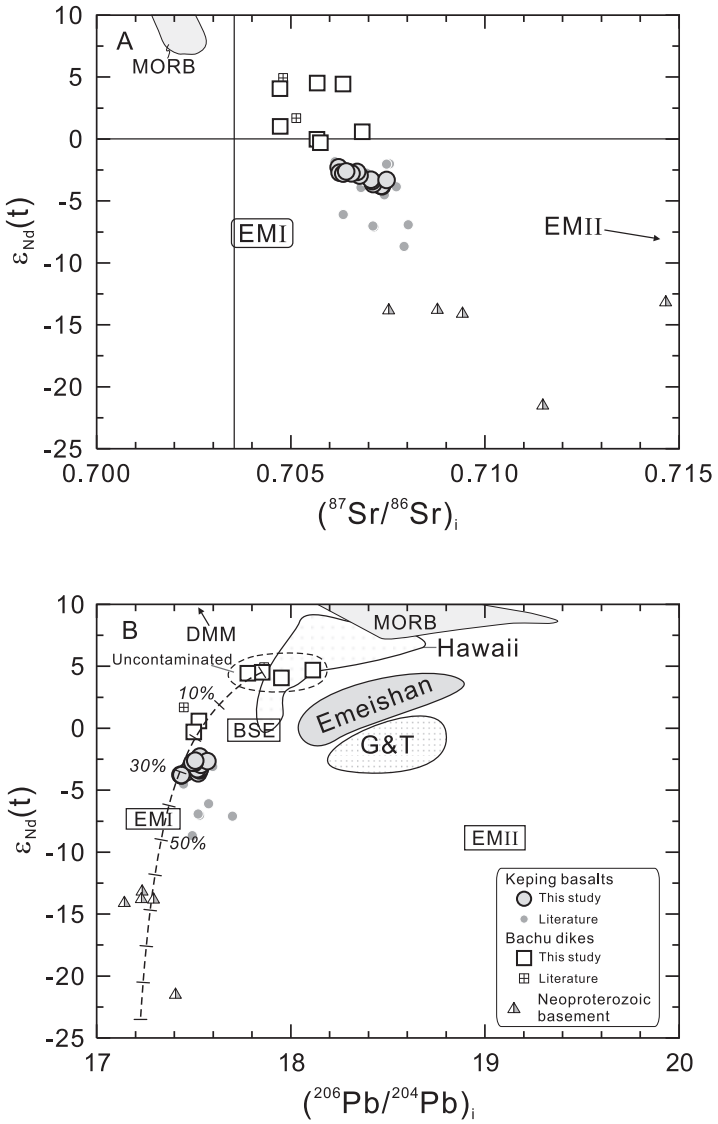

Fig. 7. Initial Sr, Nd, and Pb isotopic compositions of the Keping basalts and Bachu dikes. Note that the Keping basalts have restricted Sr-Nd-Pb isotopic compositions distinct from those of the Bachu dikes. Dashed outlined field highlights uncontaminated samples from the Bachu dikes (see "crustal contamination" section for details). Dashed lines are mixing curves with tick marks at 10% for a sample from the Bachu dikes (BC-4) with 32.7 ppm Nd, $\varepsilon_{Nd}(280)$ of 4.5, 3.81 ppm Pb, $(^{206}Pb/^{204}Pb)_i$ of 17.853. End-member utilized is Neoproterozoic igneous rocks with 26.0 ppm Nd, $\varepsilon_{Nd}(280)$ of −23.6, 18.6 ppm Pb, $(^{206}Pb/^{204}Pb)_i$ of 17.226 (Cao and others, 2011). In Pb-Pb isotope space, the Northern Hemisphere Reference Line (NHRL; Hart, 1984) is shown. Approximate locations of mantle end-members (Zindler and Hart, 1986) are indicated for reference. Also shown are the fields of Emeishan least contaminated high-Ti basalts, western China (Xu and others, 2001; Xiao and others, 2004; Zhang and others, 2006; Qi and Zhou, 2008), Hawaiian OIB and Gough and Tristan (G&T) (http://georoc.mpch-mainz.gwdg.de/georoc/). Literature data sources same as in figure 3.

Bachu dikes.—Due to disturbed Ar systematics caused by severe alteration (see LOI in table 2; see also Zhang and others, 2010c, alteration effects), most of the $^{40}Ar/^{39}Ar$ results published cannot be utilized to constrain the age of the mafic dikes because the

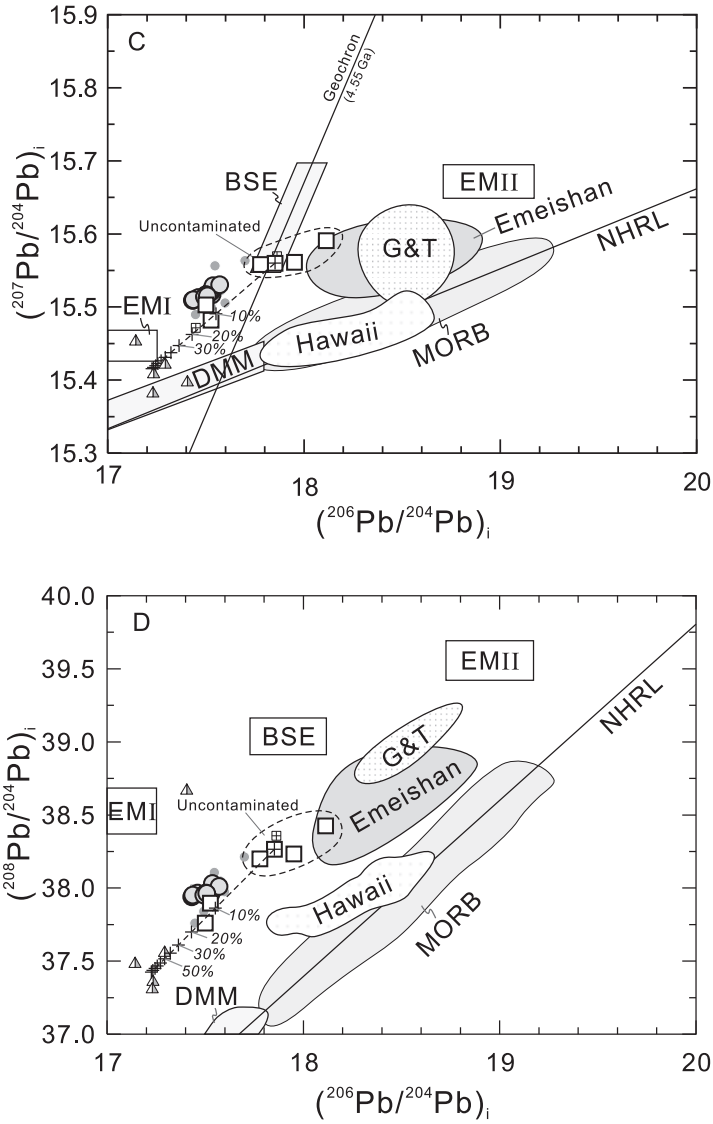

Fig. 7 (continued).

plateau ages often contain less than 40 percent of the total ^{39}Ar released and are mostly discrepant with the inverse isochron ages (Zhang and others, 2010c).

Mafic dikes around the Xiaohaizi syenite complex intrude the Silurian-early Permian strata (fig. 1C). These mafic dikes also intrude the Xiaohaizi syenite complex and Wajilitag ultramafic-mafic-felsic layered intrusion with some of them intermingling with the syenite (Zhang and others, 2008b, 2010b; Chen and others, 2010). Therefore, the mafic dikes are coeval to the Xiaohaizi syenite and Wajilitag layered intrusion. Zircon U-Pb dating of the Xiaohaizi syenite complex yielded ages ranging from 277.0 ± 4.0 Ma to 282.0 ± 3.0 Ma (2σ; Yang and others, 2006b; Li and others, 2007; Zhang and others, 2009b, 2010b; Wei and Xu, 2011) and a weighted mean

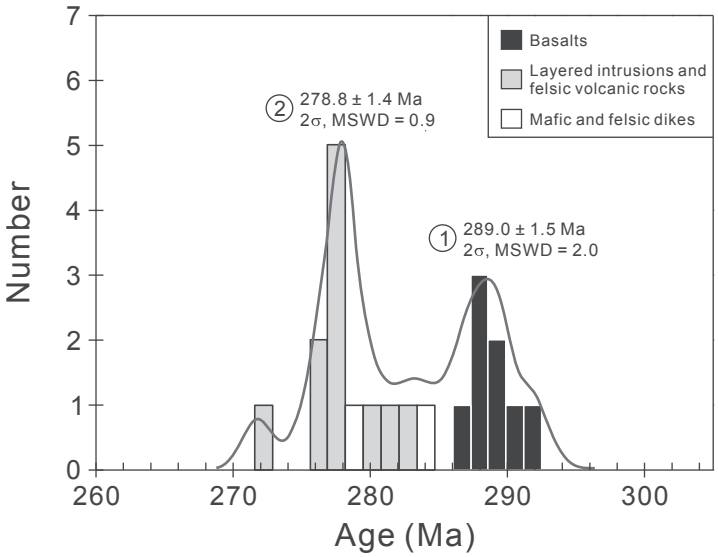

Fig. 8. Compilation of reliable $^{40}Ar/^{39}Ar$ and zircon U-Pb ages of the Tarim basalts, ultramafic-mafic-felsic intrusions, mafic and felsic dikes and rhyolites. The numbers at the peaks of probability curves (289 Ma and 279 Ma) represent the averaged ages of both literature data and those reported in this study. Data sources: Yang and others, 1996, 2006b; Li and others, 2007, 2011; Zhang and others, 2008a, 2009b, 2010b, 2012b; Yu, ms, 2009; Tian and others, 2010; Shangguan and others, 2011; Wei and Xu, 2011; Yu and others, 2011a, 2011b and this study.

$^{206}Pb/^{238}U$ age of 279.0 ± 1.9 Ma (2σ, n = 5) has been taken as the crystallization age of the Xiaohaizi syenite complex.

In addition to the mafic dikes, quartz syenite porphyries are also widely distributed in the Xiaohaizi and Wajilitag areas and intrude the Xiaohaizi syenite and Wajilitag layered intrusion (BGMRXUAR, 1993; Zhang and others, 2008b, 2010b; Chen and others, 2010), which could be used to place better constraints on the age of the dikes. The porphyries crosscutting the sedimentary strata yielded SHRIMP zircon U-Pb ages of 278.4 ± 2.2 Ma (2σ; Yu, ms, 2009) and 284.3 ± 2.8 Ma (2σ; Li and others, 2011), indicating that the quartz syenite porphyries could have formed between 278 and 284 Ma. Thus, the published ages suggest that the intrusions and dikes could have been emplaced over a long time interval, between 277.0 and 284.3 Ma.

Summary–two main magmatic episodes of magmatism in the TLIP.—Careful screening of dates available in literatures delineates two main magmatic episodes in the TLIP. The distribution of ages reported in the literature together with those obtained in this study clearly defines two statistically significant age groups (fig. 8). The earlier episode, characterized by flood basaltic volcanism, formed at 286 to 292 Ma, and peaked at 289.0 ± 1.5 Ma (2σ; fig. 8). The later episode is marked by ultramafic-mafic-felsic layered intrusions and felsic volcanic rocks and some mafic and felsic dikes in Bachu, Piqiang and the northern Tarim Craton along the margins. These rocks were emplaced over a 12 Ma time interval, between 271.7 to 284.3 Ma, with the main pulse at 277 to 284 Ma and peaked at 278.8 ± 1.4 Ma (2σ; fig. 8). However, the current geochronological data do not permit close resolution of the duration of a single igneous pulse, which awaits acquisition of high-precision IDTIMS (isotope dilution thermal ionization mass spectrometry) U-Pb analyses on single zircon crystals of the Tarim basalts and Bachu intrusions and dikes (Luo and others, in preparation).

Petrogenesis

Effect of alteration.—The effects of alteration on the geochemistry of the Keping basalts appear to be minor, given the relatively low LOI (0-1.7 wt.%; table 2). This is further supported by good correlations between Y, Nb, Ba, Lu, U and Zr, which is generally considered to remain inert during alteration/weathering (Winchester and Floyd, 1977) (fig. 6). Whereas, Rb is not correlated with Zr (fig. 6A), indicating that Rb has been affected by alteration/weathering for the Keping basalts. In contrast, the Bachu dikes have relatively higher LOI (1.8-4.2 wt.%; table 2) and show petrographic evidence of alteration with clinopyroxene transformed to magnetite. The negative correlations of Na_2O, K_2O and Rb with LOI (not shown) suggest the loss of these elements during alteration/weathering. The lack of correlation between Rb, Ba and Zr (fig. 6A and D) indicates the mobility of Rb and Ba. Whereas, Y, Nb, Lu, U show positive correlations with Zr, suggesting that these elements were relatively immobile. Rb was mobile for both the Keping basalts and Bachu dikes, thus the age-corrected $^{87}Sr/^{86}Sr$ based on Rb/Sr ratios of the measured samples hardly reflect that of mantle source.

There is a weak positive correlation between $(^{206}Pb/^{204}Pb)_i$ and LOI (fig. 9B) for the Keping basalts. A similar correlation is found between $(^{143}Nd/^{144}Nd)_i$ and LOI (fig. 9A), which cannot be attributed to alteration. For the Bachu dikes, Nd and Pb isotopic ratios do not correlate with each other (fig. 9). The samples with the lowest $(^{206}Pb/^{204}Pb)_i$ also have lower $(^{143}Nd/^{144}Nd)_i$, indicative of the effect of possible crustal assimilation (see below) rather than alteration.

Crystal fractionation.—The low MgO (4.3-5.9 wt.%), Mg# (32-42) and Ni contents (3.1-77.8 ppm) indicate that the Keping basalts underwent extensive fractional crystallization of ferromagnesian minerals and plagioclase. For example, positive trends of Al_2O_3-MgO (fig. 4B) and Al_2O_3-CaO (fig. 4F) and relative depletion in Sr (fig. 5B) are consistent with fractionation of plagioclase, in agreement with the presence of plagioclase phenocrysts in some samples. TiO_2 and Fe_2O_3T correlate negatively with MgO (figs. 4A and 4C), arguing against significant fractionation of Fe-Ti oxides. Significant clinopyroxene fractionation is not possible given the lack of correlation between MgO and CaO (fig. 4D).

In contrast, the Bachu dikes show a systematic decrease in TiO_2, Fe_2O_3T and CaO (figs. 4A, 4C, and 4D), and an increase in Al_2O_3 (fig. 4B) with decreasing MgO, consistent with fractionation of olivine, clinopyroxene and Fe-Ti oxides and negligible plagioclase. The Fe-Ti oxide fractionation is further confirmed by the extremely low Cr content (0.08-0.69 ppm) displayed by the majority of the Bachu dikes ($K_D^{magnetite/melt}$ Cr = 50-230; Leeman and others, 1978).

It seems that the Keping basalts and Bachu dikes experienced different fractionation processes. This, together with their distinct compositional variations (fig. 4), suggests that the Keping basalts and Bachu dikes cannot be related by crystallization along a single liquid line of descent from a common parental magma.

Crustal contamination.—The Keping basalts and Bachu dikes display distinct Sr-Nd-Pb isotope compositions, reflecting variable contributions from different mantle and/or crustal components. The upper crust in Tarim is dominated by Archean gneisses reworked during the Proterozoic and Neoproterozoic (Hu and others, 2000; Xu and others, 2005; Zhang and others, 2007, 2012a; Long and others, 2010, 2011; Cao and others, 2011; Zhu and others, 2011). The Archean and Neoproterozoic basements are characterized by low ε_{Nd} (−12 to −37, corrected to 290 Ma). No Pb isotopic data are available for the Archean basement, but $^{206}Pb/^{204}Pb$ of the Neoproterozoic basement is low (17.14-17.41) (Cao and others, 2011). Contamination/assimilation of mantle-derived magmas by such crustal contaminants would drive the magma composition towards low $\varepsilon_{Nd}(t)$ and crust-like trace element ratios. Both trace element data

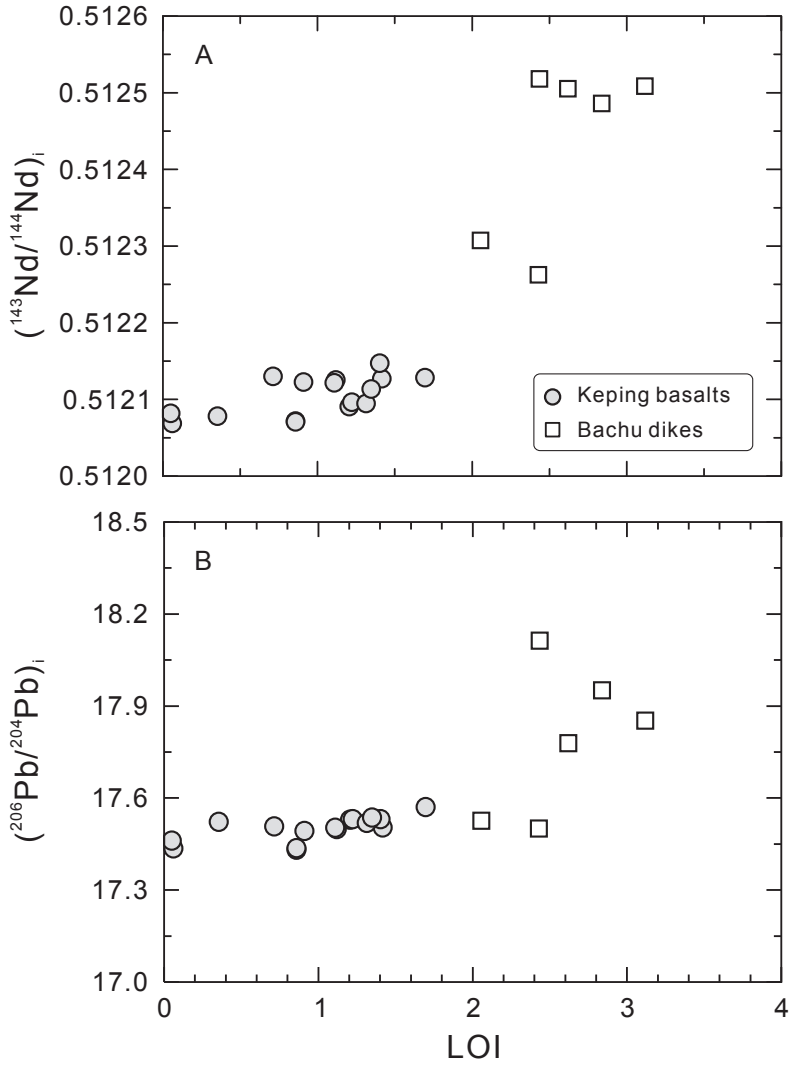

Fig. 9. $(^{143}Nd/^{144}Nd)_i$ and $(^{206}Pb/^{204}Pb)_i$ versus LOI.

and isotopic compositions are utilized to investigate whether the Keping basalts were derived from a mantle source similar to the Bachu dikes, subsequently contaminated by continental crust during magma ascent.

This petrogenetic model has been invoked by Zhou and others (2009) to account for the enriched Nd isotopic compositions [$\varepsilon_{Nd}(t) = -2.66$ to -9.27] of the Keping basalts. The involvement of crustal materials in the genesis of the Keping basalts is possible given their slightly lower Nb/U (25.9-37.9) and Ce/Pb (11.8-16.4) ratios with respect to mid-ocean ridge basalts (MORB) and OIB (Nb/U = 52 ± 15, Ce/Pb = 25 ± 5; Hofmann and others, 1986; Hofmann, 2003). However, to explain the Pb compositions solely by assimilation of an OIB-like composition with upper continental crust (average Pb concentration ~17 ppm; Rudnick and Gao, 2003), large amounts of assimilated material (up to 24%) would be required (fig. 10A), given the moderate Pb

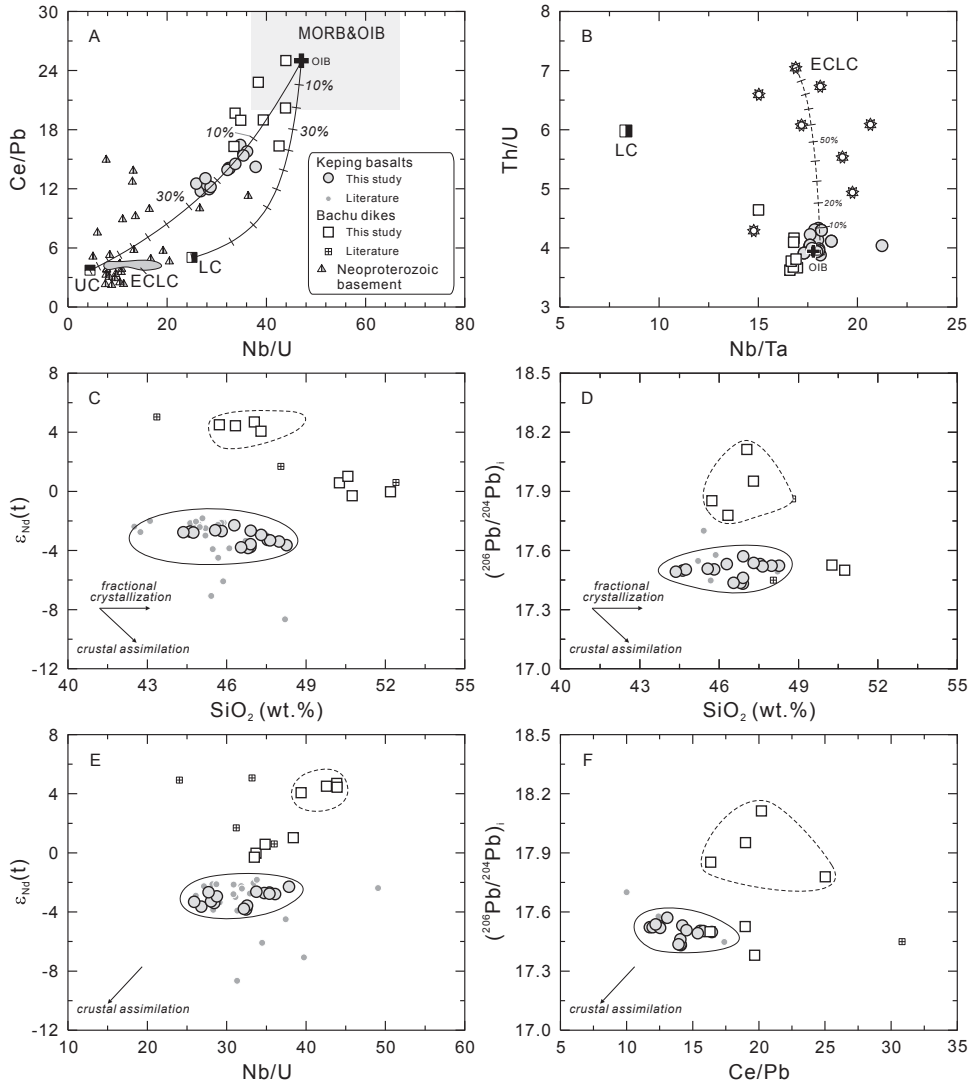

Fig. 10. Plots of Ce/Pb versus Nb/U (A), Th/U versus Nb/Ta (B), $\varepsilon_{Nd}(t)$ versus SiO_2 (C) and $(^{206}Pb/^{204}Pb)_i$ versus SiO_2 (D), $\varepsilon_{Nd}(t)$ versus Nb/U (E) and $(^{206}Pb/^{204}Pb)_i$ versus Ce/Pb (F) to assess the effect of crustal assimilation on the compositions of the Keping basalts and Bachu dikes. Arrows indicate different magma variation trends (see text for explanation). Solid and dashed outlined fields highlight that these samples display trends parallel to that of the fractional crystallization and thus are not affected by shallow-level crustal assimilation (see text for details). (C-F) initial Nd and Pb isotopes versus SiO_2, Nb/U and Ce/Pb, illustrate that in contrast to the Keping basalts, some Bachu dikes that deviate from the dashed outlined field were modified to a significant degree by crustal assimilation (see arrows). In figure 10A, black curved lines with tick marks represent binary mixing between an average oceanic island basalt (OIB; Sun and McDonough, 1989) and the average continental upper (UC) and lower crust (LC) (Rudnick and Gao, 2003). The gray fields of oceanic basalts (MORB and OIB), and the lower crust of the East China (ECLC) represent the Ce/Pb and Nb/U values taken from Hofmann and others (1986) and Gao and others (1998), respectively. In figure 10B, dashed line with tick marks represents binary mixing between a sample (23.9 ppm Nb, 1.32 ppm Ta, 3.34 ppm Th and 0.86 ppm U) from the Keping basalts with Th/U and Nb/Ta ratios similar to OIB and primitive mantle (Sun and McDonough, 1989) with an average lower crust of the East China (ECLC) (10.0 ppm Nb, 0.59 ppm Ta, 9.23 ppm Th and 1.31 ppm U; Gao and others, 1998). Neoproterozoic basements from Cao and others (2011), Long and others (2011) and Zhu and others (2011). Literature data sources same as in figure 3.

concentrations in the Keping samples (5.2-7.1 ppm). This is not in agreement with the trace element budget and the Nd isotope systematics. Moreover, such a high amount of crustal assimilation could significantly change major element compositions of resultant magmas, making them no longer basaltic in nature. A significant role for shallow-level crustal assimilation during the petrogenesis of the Keping basalts can thus be ruled out, because (a) the samples show limited range in Nd and Pb isotope composition and of ratios such as Th/Nb and Nb/La that sensitive to crustal assimilation (figs. 7, 11A and 11B); (b) neither $\varepsilon_{Nd}(t)$ nor $(^{206}Pb/^{204}Pb)_i$ correlate with SiO_2, Nb/U and Ce/Pb (figs. 10C, 10D, 10E and 10F).

While assimilation of the upper crust can be precluded, the contribution of lower crust material more mafic in composition to magma genesis needs to be assessed. Unfortunately, the nature of the lower crust beneath Tarim remains largely unknown. The Tarim Craton has an Archean and Proterozoic basement (BGMRXUAR, 1993; Hu and others, 2000; Xu and others, 2005, 2009; Zhang and others, 2007, 2012a; Lu and others, 2008; Long and others, 2010, 2011; Cao and others, 2011; Zhu and others, 2011) and extremely weak magmatism occurred between Proterozoic and early Permian (BGMRXUAR, 1993; Zhang and others, 2013). It is therefore possible that the Tarim lower crust was formed during Archean and Proterozoic and may have element and isotopic compositions similar to the Archean/Proterozoic lower crust elsewhere. Basaltic underplating at the base of the crust has been emphasized as a mechanism for generating the mafic lower crustal granulite xenoliths, providing heat for granulite-facies metamorphism (for example, Rudnick and others, 1986; Downes and others, 1990; Rudnick, 1990). For the purpose of this study, the lower crust beneath North China is used in evaluation.

On the plots of Th/U versus Nb/Ta (fig. 10B), $(Nb/Zr)_{PM}$ and $(La/Nb)_{PM}$ versus $(Th/Nb)_{PM}$ (figs. 11A and 11B), the Keping basalts display trends towards the lower crust. The variable ranges of Th/U, Th/Nb and La/Nb can be explained by mixing ~10 percent of a sample with the highest ratios similar to OIB and the primitive mantle with an average composition of the lower crust beneath North China (Gao and others, 1998) (figs. 10B, 11A and 11B). If a more primitive composition with lower element concentration were chosen, the proportion would be considerably lower. The lower crustal contamination could also drive the magma composition towards low $\varepsilon_{Nd}(t)$ and $(^{206}Pb/^{204}Pb)_i$, given low $^{206}Pb/^{204}Pb$ ratios (13.55-16.68, calculated to 290 Ma, Cohen and others, 1984; Leeman and others, 1985; Yang and Li, 2008) and ε_{Nd} (−11 to −48, calculated to 290 Ma, Huang and others, 2004; Liu and others, 2004; Jiang and others, 2013) of Archean/Proterozoic granulite xenoliths. The lack of correlations between $\varepsilon_{Nd}(t)$ and Nb/U, and $(^{206}Pb/^{204}Pb)_i$ and Ce/Pb (figs. 10E and 10F) argue against significant lower crustal assimilation. Overall, lower crustal assimilation may have exerted a restricted effect on the Keping basalts, but did not significantly change their compositions. Consequently, their low Nb/U, Ce/Pb and isotopic signatures largely reflect those of mantle sources.

Most of the Bachu dikes have relatively high Nb/U (39.4-43.9), Ce/Pb (19-25.6), Nb/La (1.1-1.4) and low Zr/Nb (5.2-6.3) ratios, and also display high $\varepsilon_{Nd}(t)$ (4.1-4.7) and $(^{206}Pb/^{204}Pb)_i$ (17.779-18.153) (figs. 10C and 10D). Therefore, these samples were not affected by crustal contamination and their trace elements and isotopic compositions could be representative of their mantle sources. In contrast, the remaining samples of the Bachu dikes have relatively low Ce/Pb (16.3-19.7) (with the exception of BC-12, Ce/Pb 22.8), Nb/U (33.5-38.4), Zr/Nb (6.5-7.0), $\varepsilon_{Nd}(t)$ (−0.3-1.0) and $(^{206}Pb/^{204}Pb)_i$ (17.500-17.526). As a whole, the Bachu dikes show negative trends in the plots of $\varepsilon_{Nd}(t)$ and $(^{206}Pb/^{204}Pb)_i$ versus SiO_2 (figs. 10C and 10D), and positive trend in the plot of $\varepsilon_{Nd}(t)$ versus Nb/U (fig. 10E). It is clear that the samples with low $\varepsilon_{Nd}(t)$ and $(^{206}Pb/^{204}Pb)_i$ have undergone significant crustal contamination.

To further test the possible influence of basement assimilation on the Bachu dikes, we use a simple bulk mixing model applied to trace element ratios and isotopes (figs. 7 and 11). It is shown that the Nd-Pb isotope compositions of the Bachu dikes can be accounted for by a mixing between an uncontaminated sample (BC-4) and a contaminant with composition similar to the Tarim Neoproterozoic basement (fig. 7). Calculation shows that to explain the trace element, Nd and Pb isotopic budget of contaminated samples from the Bachu dikes, up to 20 percent contamination is required (figs. 7 and 11). If an uncontaminated end member with a primitive composition (low incompatible trace element composition) is chosen, the proportion of crustal contamination would be considerably lower.

Partial melting.—One of the salient differences between the Keping basalts and Bachu dikes is their contrasting trace element patterns (fig. 5), best illustrated by the MREE/HREE fractionation systematics. Whereas LREE/MREE ratios (for example, La/Sm) largely overlap between the two groups, the MREE/HREE ratios of the Bachu dikes are systematically higher [$(Sm/Yb)_N$ = 4.1-4.9] than those of the Keping basalts [$(Sm/Yb)_N$ = 2.6-3.1]. The high La/Yb relative to Tb/Yb for these lavas suggests an origin involving partial melting of an LREE-enriched mantle source.

The elevated HREE concentrations and flat HREE patterns displayed by the Keping basalts [$(Dy/Yb)_N$ = 1.36-1.48; fig. 5A] cannot be simply explained by minor amount (2-3%, fig. 12) of residual garnet in the mantle source. There is increasing evidence that erupted basalts at the surface may represent a mixture of melt fractions derived from mantle sources at variable depths (Kamenetsky and others, 2012; Kuang and others, 2012; Huang and others, 2013). The strong garnet signature would have been diluted by mixing with melts from shallower depths. The evidence for this interpretation is that Sm/Yb ratios (2.4-2.9) show relatively large variability, whereas La/Sm ratios (3.8-3.9) are constant. The Keping basalts lie along the mixing curve between melt derived from ~5 percent melting of a source with 2 percent residual garnet, and from ~6 percent melting of a source with 7 percent residual garnet (fig. 12A). When plotted on the Tb/Yb versus La/Yb diagram (fig. 12B), a similar result can also be obtained. This indicates that the Keping basalts may be a mixture of melts derived from different depths of a LREE-enriched mantle source. The high level of MREE/HREE enrichment of the Bachu dikes can be attributed to large amount (5-7%) of residual garnet in their mantle source (fig. 12).

Contrasting Mantle Sources for the Keping Basalts and Bachu Dikes

Lithospheric involvement in the Keping basalts.—The Keping basalts have relatively high Ba and Pb abundances associated with negative Nb and Ta anomalies (fig. 5B), in contrast with oceanic basalts (OIB and MORB; figs. 11A and 11B), but resemble many CFBs and volcanic arc basalts. As discussed previously, crustal contamination appears to be negligible and thus it may not exert a significant role in the generation of this crustal signature. If we accept this feature to be diagnostic of the mantle source, then an SCLM source metasomatized by (subduction-related?) silicate melts or fluids is implied. A similar petrogenetic model has widely been proposed for many CFBs (Hergt and others, 1991; Lightfoot and others, 1993; Turner and Hawkesworth, 1995; Frey and others, 1996; Garland and others, 1996; Peate and Hawkesworth, 1996; Xiao and others, 2004).

Thermomechanic modeling suggests that substantial melting, as would be required to produce CFBs, of the SCLM appears to be unlikely if the mantle is initially cold and dry (Arndt and Christensen, 1992), but is theoretically possible if the mantle is previously hydrated by volatiles and melts when conductively heated from below by an upwelling plume (Gallagher and Hawkesworth, 1992; Turner and others, 1996). There is increasing evidence that continental basalts associated with Archean lithosphere have EM1 or extreme EM1 isotopic signatures, such as the Cenozoic Wyoming-

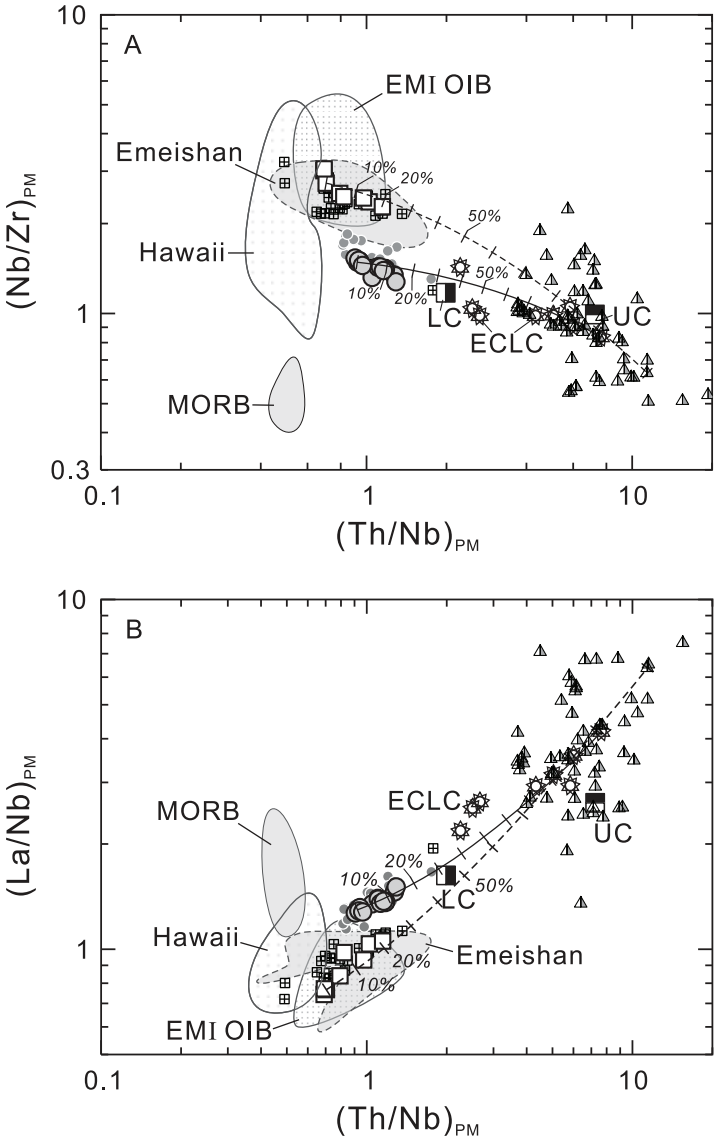

Fig. 11. Plots of $(Nb/Zr)_{PM}$ versus $(Th/Nb)_{PM}$ (A), $(La/Nb)_{PM}$ versus $(Th/Nb)_{PM}$ (B), $\varepsilon_{Nd}(t)$ versus La/Nb (C) and $(^{206}Pb/^{204}Pb)_i$ versus La/Nb (D) for the Keping basalts and Bachu dikes. In figure A and B, subscript PM indicates ratios normalized to primitive mantle values of McDonough and Sun (1995). Results are shown for assimilation of a sample from the Keping basalts (YG-7) and an uncontaminated sample from the Bahcu dikes (BC-4) with an average ECLC and the Neoproterozoic igneous rocks, respectively. Solid and dashed curves with tick marks at 10% indicate the amount of assimilated material relative to YG-7 and BC-4, respectively. The average ECLC is modeled with 9.23 ppm Th, 10.0 ppm Nb, 191 ppm Zr and 41.3 ppm La (Gao and others, 1998) and the Neoproterozoic igneous rocks with 9.21 ppm Th, 6.7 ppm Nb, 169 ppm Zr, 42.0 ppm La, 26.0 ppm Nd, $\varepsilon_{Nd}(280)$ of −23.6, 18.6 ppm Pb and $(^{206}Pb/^{204}Pb)_i$ of 17.226 (Zhang and others, 2007; Cao and others, 2011). Data sources: EMI OIB (including Wavis Ridge, Gough and Tristan) from Willbold and Stracke (2006), Class and le Roex (2008); Salters and Sachi-Kocher (2010); Emeishan least contaminated high-Ti basalts and Hawaiian OIB same as figure 7. Literature data sources same as in figure 3.

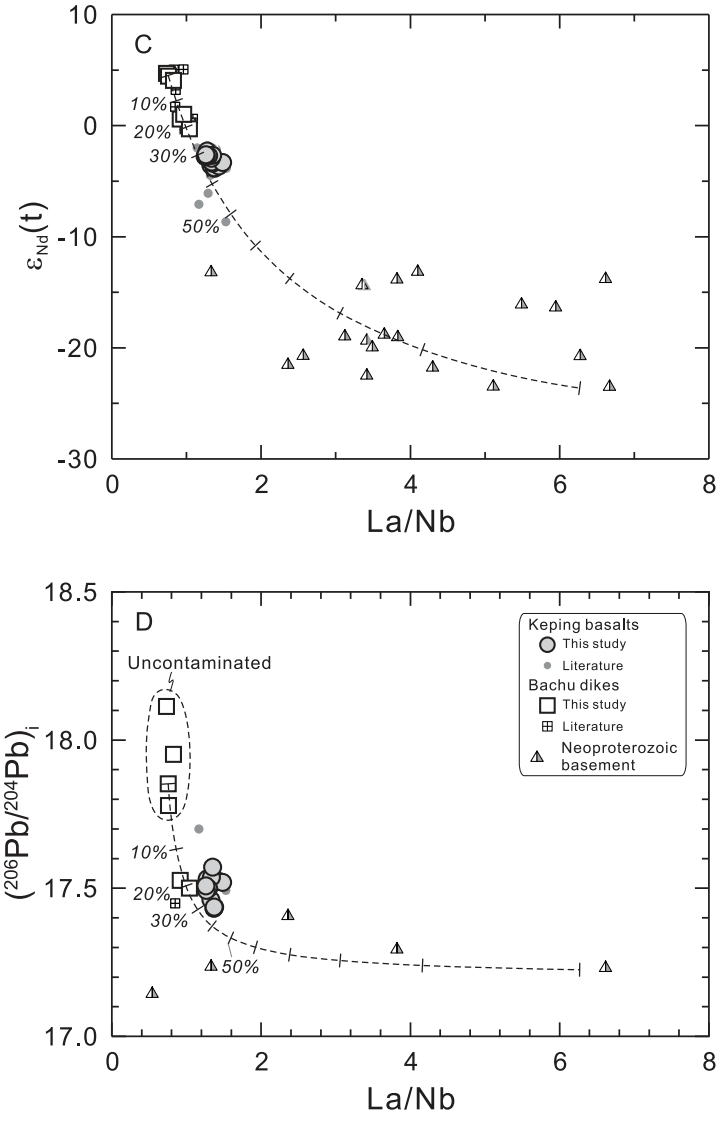

Fig. 11 (continued).

Montana alkaline province in western North America (Greenough and Kyser, 2003; Greenough and others, 2005, 2007) and the Suwar intrusion, in Yemen (Greenough and others, 2011). This suggests that the ancient SCLM could be inevitably modified by later stage subduction processes. The SCLM is often modified by fluids related to dehydration or sediment melting in subduction zones (Noll Jr. and others, 1996; Johnson and Plank, 2000; Class and others, 2000) and may have incorporated subducted sediments (Ben Othman and others, 1989; Sun and others, 1989). Tarim has a long history of subduction, which could have modified the SCLM. The northern margin of the Tarim Craton may have witnessed two major orogenic events, a Paleoproterozoic orogeny (*ca.* 2.0-1.8 Ga) coincident with the timing of the orogeny

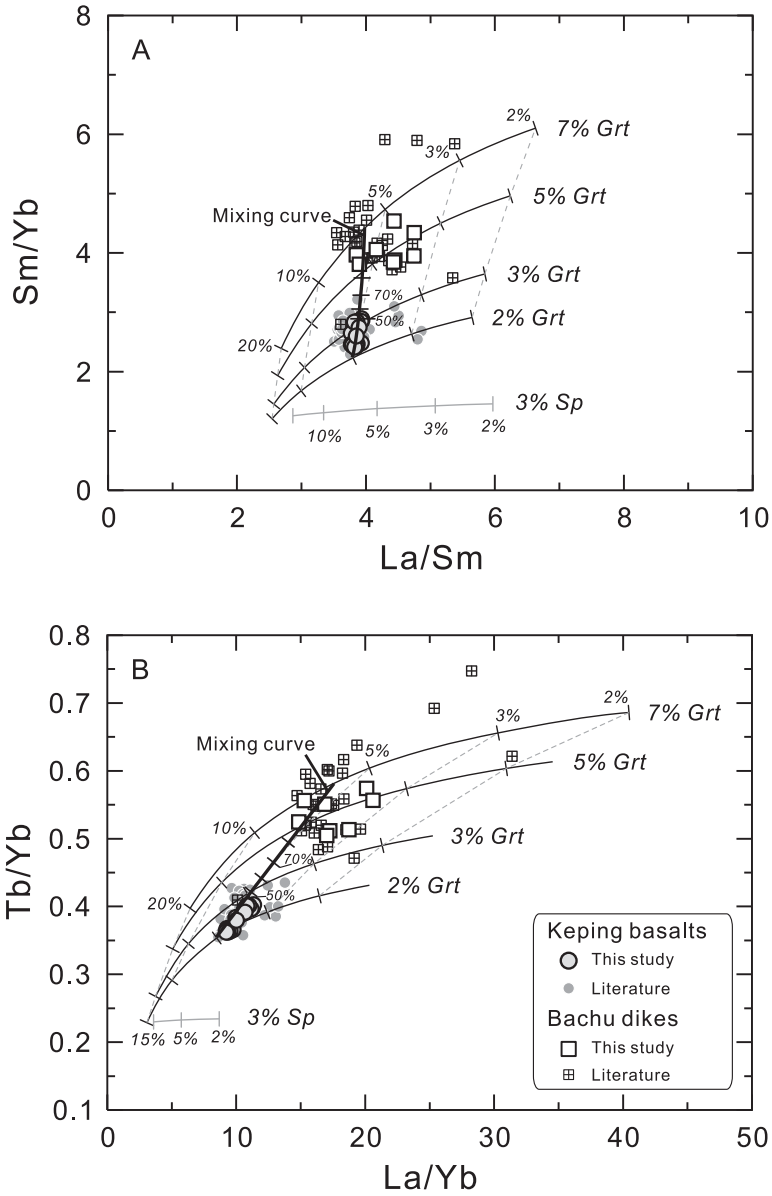

Fig. 12. (A) Sm/Yb versus La/Sm and (B) Tb/Yb versus La/Yb for the Keping basalts and Bachu dikes and non-modal batch melting (Shaw, 1970) of a lherzolitic mantle source highlighting the role of garnet and spinel in the melting region. Partition coefficients are from McKenzie and O'Nions (1991). The tick marks on the curves correspond to melting degrees. Gray curves: melting curve of a spinel-bearing lherzolite source (modal composition and melt mode of 53% olivine, 27% orthopyroxene, 17% clinopyroxene, 3% spinel and −6% olivine, 28% orthopyroxene, 67% clinopyroxene, 11% spinel, respectively; Kinzler, 1997). Black curves: melting curves of garnet-bearing lherzolite mantle sources containing varying modal garnet (59-64% olivine, 21% orthopyroxene, 13% clinopyroxene, 7-2% garnet and 4% olivine, −19% orthopyroxene, 104% clinopyroxene, 11% garnet, respectively; Hellebrand and others, 2002). The heavy lines represent mixing curves between melt derived from 5% melting of a source with 2% residual garnet and from 6% melting of a source with 7% residual garnet. Source composition: 1.45 ppm La, 0.52 ppm Sm, 0.099 ppm Tb and 0.441 ppm Yb. The assumed source is "97.4% primitive mantle (McDonough and Sun, 1995) + 2.6% upper crust (Rudnick and Gao, 2003)," except for Tb and Yb (McDonough and Sun, 1995) to fit the requirement of a similar LREE-enriched source for the two groups. If Tb and Yb are also enriched by the addition of crustal materials, a slightly higher Tb/Yb (0.239) ratio of the source will be obtained and melt derived from this mantle source will also have slightly higher Tb/Yb ratio. Therefore, smaller amount of residual garnet in the source will be required for the Keping basalts. Literature data sources same as in figure 3.

associated with the assembly of the Columbia supercontinent (Zhu and others, 2011) and a Tarimian orogeny (*ca.* 1.05-0.90 Ga) which resulted in the final cratonization of Tarim (Zhang and others, 2007, 2011; Lu and others, 2008; Cao and others, 2011; Ge and others, 2012; He and others, 2012). During these orogenies, an active continental margin may have existed along the northern margin of the Tarim Craton (Liou and others, 1996; Zhang and others, 2009a; Zhu and others, 2011). On the other hand, the Tarim Craton was amalgamated to the CAOB in the late Carboniferous indicated by the West Tianshan high to ultrahigh pressure metamorphic rocks including coesite-bearing eclogites (Lü and others, 2008; Han and others, 2011). The crustal materials could have been recycled into the SCLM during continental deep subduction, and the SCLM may also have been metasomatized by silicate melts derived from subducted continental crust (Jahn and others, 1999; Zheng and others, 2009; Dai and others, 2011, 2012; Zhao and others, 2012; Zheng, 2012).

Contribution of sediments to the mantle source of the Keping basalts is evident from the correlation between Th/Yb, $\varepsilon_{Nd}(t)$ and Ba/La (fig. 13), because these variables are reliable indicators of potential sediment or fluid contributions to magma source regions (Woodhead and others, 2001). The Keping basalts have low $\varepsilon_{Nd}(t)$ values (-2.3 to -3.8), very unradiogenic $(^{206}Pb/^{204}Pb)_i$ ratios (17.4 to 17.6), and low $(^{208}Pb/^{204}Pb)_i$ ratios ($\sim$38.0). These imply a source with low time-integrated Sm/Nd and U/Pb, coupled with relatively low Th/U ratios. Such elemental fractionations are characteristic of average pelagic sediments reported by Plank and Langmuir (1998) which has Sm/Nd = 0.21 and Th/U = 4.11, similar to typical upper continental crustal values (Sm/Nd = 0.17, Th/U = 3.89; Rudnick and Gao, 2003).

Hf and Nd isotope systematics are effective in identifying and distinguishing upper continent-derived materials from pelagic sediments (Vervoort and others, 1999; Eisele and others, 2002). Hf and Nd isotopic compositions are highly correlated in crustal materials as a whole, with regression line slopes in ε_{Hf}–ε_{Nd} space being around 1.5 (Chauvel and others, 2008; Vervoort and others, 2011). Pelagic sediments, however, are an exception to this probably due to the lack of a zircon-hosted Hf component resulting in generally higher Lu/Hf ratios (Patchett and others, 1984; Vervoort and others, 1999, 2011). Therefore, magmas derived from sources with recycled pelagic sediments would have regression line slopes in ε_{Hf}–ε_{Nd} space significantly lower than the terrestrial mantle array (Eisele and others, 2002; Marini and others, 2005). The Keping basalts form a good positive correlation between $\varepsilon_{Hf}(t)$ and $\varepsilon_{Nd}(t)$ with a slope of $\sim$1.5 similar to that of terrestrial mantle array (Li and others, 2012b), indicating that upper continental-derived materials mainly from continental margins rather than pelagic sediments were involved in their source.

Plume signature in the Bachu dikes.—The Bachu dikes show incompatible trace element patterns prominently similar to those of OIB (figs. 5C and 5D) and the uncontaminated samples exhibit trace element ratios that completely overlap the fields of OIB and Emeishan least contaminated high-Ti basalts from the ELIP, but distinct from MORB (figs. 11A and 11B). They also show trace element ratios (for example, Nb/La = 1.21-1.37) and Nd isotopes [$\varepsilon_{Nd}(t)$ = 4.1-4.8], similar to the proposed plume component [Nb/La = 1.0-1.1, $\varepsilon_{Nd}(t)$ = 4.6-4.8] for the Emeishan high-Ti basalts (Xu and others, 2001). The Pb isotopes overlap or are slightly lower than those of the Emeishan least contaminated high-Ti basalts (figs. 7C and 7D). These features suggest that the Bachu dikes were likely derived from a convective mantle source.

In the Bachu and Piqiang areas, the mafic dikes are often temporally and spatially associated with the ultramafic-mafic layered intrusions, syenites and A-type granites. In terms of isotopic similarity, these A-type granitoids share the same source with the mafic dikes and ultramafic-mafic layered intrusions (Zhang and others, 2008a, 2010b;

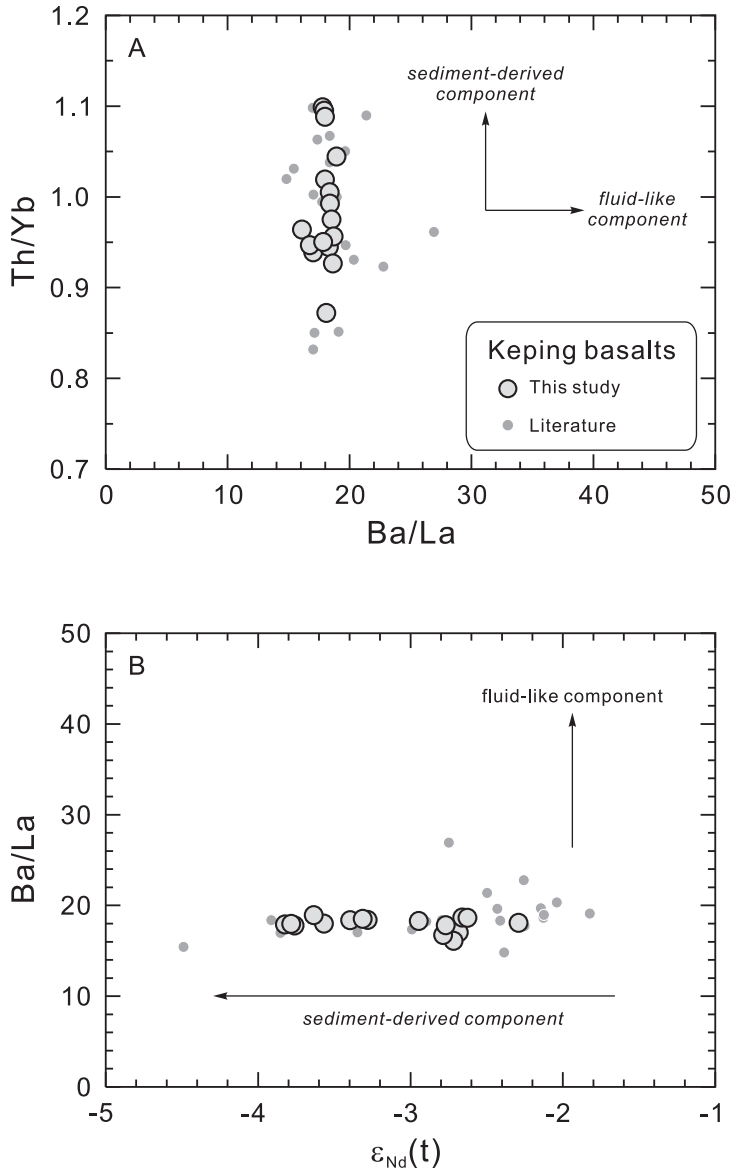

Fig. 13. The role of fluids and sedimentary components in the petrogenesis of the Keping basalts. Th/Yb versus Ba/La (A) and Ba/La versus $\varepsilon_{Nd}(t)$ (B) indicate that the compositions of the Keping basalts are controlled by sediment-derived component. Literature data sources same as in figure 3.

Wei and Xu, 2011). They have very high zircon saturation temperature (890 °C to 1010 °C; Zhang and others, 2010b), a feature of plume-related intrusions (Shellnutt and Zhou, 2007; Zhong and others, 2007, 2011; Zhong and Xu, 2009; Shellnutt and Jahn, 2010).

Plume-lithosphere interaction in the generation of the TLIP.—Any geodynamic model to be proposed should be able to account for the following main characteristics of the TLIP: (a) two magmatic episodes (~289 Ma and ~279 Ma); (b) distinct sources of

these two magmatic suites, with the earlier from the SCLM and the later possibly from a mantle plume; (c) spatial distribution of these two episodes of magmatism, with the earlier episode covering all the Tarim Craton and the later one largely confined in the periphery of the Tarim Craton. In order to fit in with the characteristics of these two discrete magmatic episodes, we propose a model involving plume-lithosphere interaction in the formation of the TLIP (fig. 14).

In this scenario, the Keping basalts are hypothesized to have formed by the arrival of a mantle plume impacting at the base of the SCLM. The Tarim Craton has a very thick SCLM more than 140 km at present (Liu and others, 2004; An and Shi, 2006; Priestley and others, 2006) and the boundaries of cratons often have relatively thinner lithosphere (for example, Lebedev and others, 2006; Shomali and others, 2006; Fishwick and others, 2008). No significant magmatic activities were observed since Permian (BGMRXUAR, 1993) indicating that Tarim might not witness obvious lithospheric thinning after Permian. Thus, it is reasonable to assume that the lithosphere of Tarim during Permian could be thicker than 140 km. A thick lithosphere (>130 km) will hamper the upwelling of a mantle plume, thus preventing its decompression melting (Davies, 1994; Sleep and others, 2002; Jourdan and others, 2007a; Foley, 2008) and melting will be confined to the lithospheric mantle (Story and others, 1997). After incubating beneath thick cratonic lithosphere (fig. 14A), the plume will be deflected away towards areas of thinner lithosphere at the craton margins (Sleep and others, 2002) and conductively heats the overlying SCLM, triggering the melting of the subduction-related metasomatized domains within the lithospheric mantle and giving rise to the Keping basalts (fig. 14B). It should be emphasized that the Keping basalts are distributed close to the margins of the Tarim Craton, where the lithosphere may be thinner than the interior of the craton. Our modeling (fig. 12) shows that the Keping basalts represent a mixture of melt fractions derived from mantle sources at variable depths. After being heated up by an incubating mantle plume for several million years, the SCLM would melt both at a deeper portion where most of the heat is accumulated and at a shallower depth due to heat penetrating by conduction. The melting mechanism of this earlier episode of magmatism in the TLIP is similar to that described by Turner and others (1996) for the Parana CFB.

The later episode of magmatism is characterized by an OIB-like geochemical signature, pointing to decompression melting of the convective mantle (fig. 14C). Lebedev and others (2006) suggested that flow of sub-lithosphere mantle from beneath cratons and the resulting decompression melting in the craton margins could explain the origin of low-volume, scattered and sporadic basalts with OIB-like signatures. The 277 to 284 Ma magmatism is characterized by low-volume and scattered basaltic dikes and is mainly distributed in the Bachu and Piqiang area along the margins of the Tarim Craton. This is actually consistent with the prediction of decompression melting of a mantle plume. The requirement for decompression melting to take place is that the lithosphere has to be thin enough (<100 km; Turner and others, 1996; Gibson and others, 2006). Since the lithosphere beneath Tarim is presently >140 km, it is reasonable to infer that the lithosphere during the early Permian was at least that thick. This means to ensure convective mantle to melt, parts of the lithosphere beneath Tarim must have been thinned to <100 km. Consequently, a delay of ~10 Ma may correspond to the time needed to thin the lithosphere. It should be pointed out that such a lithospheric thinning did not occur within the interior of the Tarim Craton, but may have been operated at contact zones between the Tianshan orogenic belt and the Tarim Craton, where rheological rupture renders thermo-mechanical erosion/removal of the lithosphere much easier than the rigid cratonic keel. Lithospheric thinning and extension may have preferentially been initiated and intensified along these weak contact zones, eventually leading to rifting

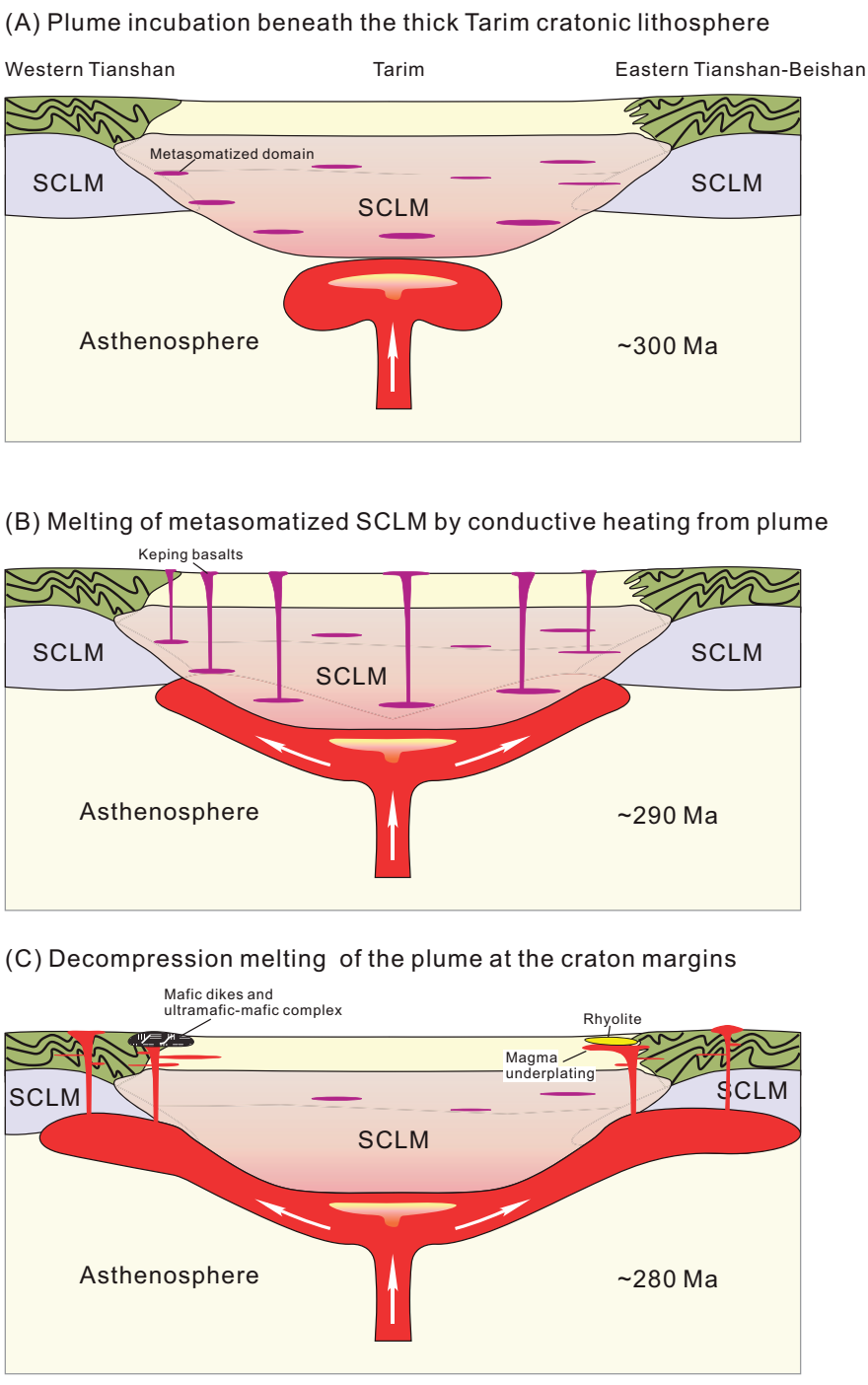

Fig. 14. A cartoon illustrating the formation of the TLIP. SCLM = subcontinental lithospheric mantle.

(Chen and others, 2009; Chen, 2010). For example, the Tanlu fault zone (TLFZ), a large trans-lithospheric strike-slip fault zone bounding the North China rift system to the east, has been proposed to operate as an asthenospheric upwelling channel and facilitate the Mesozoic–Cenozoic lithospheric thinning of the eastern North China Craton (Xu, 2001; Xu and others, 2004b; Zheng and others, 2008).

In some instances, the crust in the craton margins can also melt as a result of temperature increase related to underplating of high temperature basaltic magmas at the crust-mantle boundary. The rhyolites in the Northern Tarim could have formed in this way (fig. 14C) (Yu and others, 2011a).

CONCLUSIONS

(1) Our new $^{40}Ar/^{39}Ar$ dates together with previous published age data reveal two main episodes of magmatism in the TLIP. The flood basalts, represented by the Keping basalts, formed at 286 to 292 Ma and peaked at ~289 Ma, about 10 Ma earlier than the mafic dikes, ultramafic-mafic-felsic complex and rhyolites.

(2) The Keping basalts display a strong lithospheric signature characterized by relative depletions in Nb-Ta, enrichment in Ba-Pb, and negative $\varepsilon_{Nd}(t)$ and low initial Pb isotopes, in sharp contrast with those of oceanic island basalts. Such a lithospheric signature cannot be attributed to shallow-level crustal assimilation; rather they more likely inherit that of the SCLM beneath Tarim, which has been metasomatized by subduction-related processes. The Bachu dikes display OIB-like geochemical characteristics, consistent with a derivation from a convective mantle source.

(3) A lithosphere-plume interaction model is proposed to explain the distinct mantle components involved in two episodes of magmatism and the tempo-spatial evolution of the TLIP. The earlier episode (that is, the Keping basalts) formed by melting of the SCLM, which was initiated by the arrival of a plume impacting at the base of the SCLM. The later episode (that is, the Bachu dikes) represents decompressional melts of a mantle plume, as a result of its lateral spread out to areas of thinner lithosphere at the craton margins.

ACKNOWLEDGMENTS

We thank C. L. Zhang and members of the NSFC-funded "plume" team for assistance in the field, Y. Liu, X. L. Tu, X. R. Liang and H. N. Qiu for technical help with diverse analyses. This research was supported by National Basic Research Program of China (2011CB808906) and GIG-CAS 135 project (Y234051001). This manuscript benefits from constructive reviews by David W. Peate, John D. Greenough, and an anonymous reviewer. Xun Wei acknowledges the support of an ARC discovery grant (DP0986542) for his visit to the University of Queensland for trace element and Sr-Nd-Pb isotopic analysis. This is contribution No IS-1743 from GIG-CAS.

REFERENCES

An, M. J., and Shi, Y. L., 2006, Review on lithospheric thickness research of the Chinese continent: Earth Science Frontiers, v. 13, p. 23–30 (in Chinese with English abstract).

Arndt, N., Chauvel, C., Czamanske, G., and Fedorenko, V., 1998, Two mantle sources, two plumbing systems: tholeiitic and alkaline magmatism of the Maymecha River basin, Siberian flood volcanic province: Contributions to Mineralogy and Petrology, v. 133, n. 3, p. 297–313, http://dx.doi.org/10.1007/s004100050453

Arndt, N. T., and Christensen, U., 1992, The role of lithospheric mantle in continental flood volcanism: Thermal and geochemical constraints: Journal of Geophysical Research, v. 97, n. B7, p. 10967–10981, http://dx.doi.org/10.1029/92JB00564

Baker, J., Snee, L., and Menzies, M., 1996, A brief Oligocene period of flood volcanism in Yemen: implications for the duration and rate of continental flood volcanism at the Afro–Arabian triple junction: Earth and Planetary Science Letters, v. 138, n. 1–4, p. 39–55, http://dx.doi.org/10.1016/0012-821X(95)00229-6

Baksi, A. K., 1994, Geochronological studies on whole-rock basalts, Deccan Traps, India: evaluation of the

timing of volcanism relative to the K–T boundary: Earth and Planetary Science Letters, v. 121, n. 1–2, p. 43–56, http://dx.doi.org/10.1016/0012-821X(94)90030-2
——— 2007, A quantitative tool for detecting alteration in undisturbed rocks and minerals—II: Application to argon ages related to hotspots: Geological Society of America, Special Papers, v. 430, p. 305–333, http://dx.doi.org/10.1130/2007.2430(16)
Ben Othman, D., White, W. M., and Patchett, J., 1989, The geochemistry of marine sediments, island arc magma genesis, and crust-mantle recycling: Earth and Planetary Science Letters, v. 94, n. 1–2, p. 1–21, http://dx.doi.org/10.1016/0012-821X(89)90079-4
BGMRXUAR (Bureau of Geology and Mineral Resources of Xinjiang Uygur Autonomous Region), 1993, Regional geology of the Xinjiang Uygur Autonomous Region: Beijing: Geological Publishing House, p. 1–468 (in Chinese).
Bryan, S. E., and Ernst, R. E., 2008, Revised definition of large igneous provinces (LIPs): Earth-Science Reviews, v. 86, n. 1–4, p. 175–202, http://dx.doi.org/10.1016/j.earscirev.2007.08.008
Campbell, I. H., 2005, Large igneous provinces and the mantle plume hypothesis: Elements, v. 1, n. 5, p. 265–269, http://dx.doi.org/10.2113/gselements.1.5.265
Campbell, I. H., and Griffiths, R. W., 1990, Implications of mantle plume structure for the evolution of flood basalts: Earth and Planetary Science Letters, v. 99, n. 1–2, p. 79–93, http://dx.doi.org/10.1016/0012-821X(90)90072-6
Campbell, I. H., Czamanske, G. K., Fedorenko, V. A., Hill, R. I., and Stepanov, V., 1992, Synchronism of the Siberian Traps and the Permian–Triassic boundary: Science, v. 258, n. 5089, p. 1760–1763, http://dx.doi.org/10.1126/science.258.5089.1760
Cao, X. F., Lu, X. B., Liu, S. T., Zhang, P., Gao, X. A., Chen, C., and Mo, Y. L., 2011, LA-ICP-MS zircon dating, geochemistry, petrogenesis and tectonic implications of the Dapingliang Neoproterozoic granites at Kuluketage block, NW China: Precambrian Research, v. 186, n. 1–4, p. 205–219, http://dx.doi.org/10.1016/j.precamres.2011.01.017
Chauvel, C., Lewin, E., Carpentier, M., Arndt, N. T., and Marini, J. C., 2008, Role of recycled oceanic basalt and sediment in generating the Hf–Nd mantle array: Nature Geoscience, v. 1, p. 64–67, http://dx.doi.org/10.1038/ngeo.2007.51
Chen, H. L., Yang, S. F., Dong, C. W., Jia, C. Z., Wei, G. Q., and Wang, Z. G., 1997a, Confirmation of Permian basite zone in Tarim Basin and its tectonic significance: Geochimica, v. 26, p. 77–87 (in Chinese with English abstract).
Chen, H. L., Yang, S. F., Dong, C. W., Zhu, G. Q., Jia, C. A., Wei, G. Q., and Wang, Z. G., 1997b, Geological thermal events in Tarim Basin: Chinese Science Bulletin, v. 42, n. 7, p. 580–584, http://dx.doi.org/10.1007/BF03182623
Chen, L., 2010, Concordant structural variations from the surface to the base of the upper mantle in the North China Craton and its tectonic implications: Lithos, v. 120, n. 1–2, p. 96–115, http://dx.doi.org/10.1016/j.lithos.2009.12.007
Chen, L., Cheng, C., and Wei, Z. G., 2009, Seismic evidence for significant lateral variations in lithospheric thickness beneath the central and western North China Craton: Earth and Planetary Science Letters, v. 286, n. 1–2, p. 171–183, http://dx.doi.org/10.1016/j.epsl.2009.06.022
Chen, M. M., Tian, W., Zhang, Z. L., Pan, W. Q., and Song, Y., 2010, Geochronology of the Permian basic-intermediate-acidic magma suite from Tarim, Northwest China and its geological implications: Acta Petrologica Sinica, v. 26, p. 559–572 (in Chinese with English abstract).
Chung, S. L., and Jahn, B. M., 1995, Plume-lithosphere interaction in generation of the Emeishan flood basalts at the Permian–Triassic boundary: Geology, v. 23, n. 10, p. 889–892, http://dx.doi.org/10.1130/0091-7613(1995)023⟨0889:PLIIGO⟩2.3.CO;2
Class, C., and le Roex, A. P., 2008, Ce anomalies in Gough Island lavas—Trace element characteristics of a recycled sediment component: Earth and Planetary Science Letters, v. 265, n. 34, p. 475–486, http://dx.doi.org/10.1016/j.epsl.2007.10.030
Class, C., Miller, D. M., Goldstein, S. L., and Langmuir, C. H., 2000, Distinguishing melt and fluid subduction components in Umnak Volcanics, Aleutian Arc: Geochemistry Geophysics Geosystems, v. 1, n. 6, p. 1–30, http://dx.doi.org/10.1029/1999GC000010
Cohen, R. S., Onions, R. K., and Dawson, J. B., 1984, Isotope geochemistry of xenoliths from East Africa: Implications for development of mantle reservoirs and their interaction: Earth and Planetary Science Letters, v. 68, n. 2, p. 209–220, http://dx.doi.org/10.1016/0012-821X(84)90153-5
Collerson, K. D., Kamber, B. S., and Schoenberg, R., 2002, Applications of accurate, high-precision Pb isotope ratio measurement by multi-collector ICP-MS: Chemical Geology, v. 188, n. 1–2, p. 65–83, http://dx.doi.org/10.1016/S0009-2541(02)00059-1
Courtillot, V., Gallet, Y., Rocchia, R., Féraud, G., Robin, E., Hofmann, C., Bhandari, N., and Ghevariya, Z. G., 2000, Cosmic markers, $^{40}Ar/^{39}Ar$ dating and paleomagnetism of the KT sections in the Anjar Area of the Deccan large igneous province: Earth and Planetary Science Letters, v. 182, n. 2, p. 137–156, http://dx.doi.org/10.1016/S0012-821X(00)00238-7
Courtillot, V., Davaille, A., Besse, J., and Stock, J., 2003, Three distinct types of hotspots in the Earth's mantle: Earth and Planetary Science Letters, v. 205, n. 3–4, p. 295–308, http://dx.doi.org/10.1016/S0012-821X(02)01048-8
Dai, L. Q., Zhao, Z. F., Zheng, Y. F., Li, Q. L., Yang, Y. H., and Dai, M. N., 2011, Zircon Hf-O isotope evidence for crust–mantle interaction during continental deep subduction: Earth and Planetary Science Letters, v. 308, n. 1–2, p. 229–244, http://dx.doi.org/10.1016/j.epsl.2011.06.001
Dai, L. Q., Zhao, Z. F., Zheng, Y. F., and Zhang, J., 2012, The nature of orogenic lithospheric mantle: Geochemical constraints from postcollisional mafic–ultramafic rocks in the Dabie orogen: Chemical Geology, v. 334, p. 99–121, http://dx.doi.org/10.1016/j.chemgeo.2012.10.009

Davies, G. F., 1994, Thermomechanical erosion of the lithosphere by mantle plumes: Journal of Geophysical Research-Solid Earth, v. 99, n. B8, p. 15709–15722, http://dx.doi.org/10.1029/94JB00119
Deniel, C., and Pin, C., 2001, Single-stage method for the simultaneous isolation of lead and strontium from silicate samples for isotopic measurements: Analytica Chimica Acta, v. 426, n. 1, p. 95–103, http://dx.doi.org/10.1016/S0003-2670(00)01185-5
Downes, H., Dupuy, C., and Leyreloup, A. F., 1990, Crustal evolution of the Hercynian belt of Western Europe: Evidence from lower-crustal granulitic xenoliths (French Massif Central): Chemical Geology, v. 83, n. 3–4, p. 209–231, http://dx.doi.org/10.1016/0009-2541(90)90281-B
Duncan, R. A., Hooper, P. R., Rehacek, J., Marsh, J. S., and Duncan, A. R., 1997, The timing and duration of the Karoo igneous event, southern Gondwana: Journal of Geophysical Research-Solid Earth, v. 102, n. B8, p. 18127–18138, http://dx.doi.org/10.1029/97JB00972
Eggins, S. M., Woodhead, J. D., Kinsley, L. P. J., Mortimer, G. E., Sylvester, P., McCulloch, M. T., Hergt, J. M., and Handler, M. R., 1997, A simple method for the precise determination of ≥40 trace elements in geological samples by ICPMS using enriched isotope internal standardisation: Chemical Geology, v. 134, n. 4, p. 311–326, http://dx.doi.org/10.1016/S0009-2541(96)00100-3
Eisele, J., Sharma, M., Galer, S. J. G., Blichert-Toft, J., Devey, C. W., and Hofmann, A. W., 2002, The role of sediment recycling in EM-1 inferred from Os, Pb, Hf, Nd, Sr isotope and trace element systematics of the Pitcairn hotspot: Earth and Planetary Science Letters, v. 196, n. 3–4, p. 197–212, http://dx.doi.org/10.1016/S0012-821X(01)00601-X
Ellam, R. M., Carlson, R. W., and Shirey, S. B., 1992, Evidence from Re-Os isotopes for plume-lithosphere mixing in Karoo flood basalt genesis: Nature, v. 359, p. 718–721, http://dx.doi.org/10.1038/359718a0
Ewart, A., Milner, S. C., Armstrong, R. A., and Duncan, A. R., 1998, Etendeka volcanism of the Goboboseb Mountains and Messum Igneous Complex, Namibia. Part I: Geochemical evidence of Early Cretaceous Tristan Plume Melts and the role of crustal contamination in the Paraná-Etendeka CFB: Journal of Petrology, v. 39, n. 2, p. 191–225, http://dx.doi.org/10.1093/petroj/39.2.191
Fishwick, S., Heintz, M., Kennett, B. L. N., Reading, A. M., and Yoshizawa, K., 2008, Steps in lithospheric thickness within eastern Australia, evidence from surface wave tomography: Tectonics, v. 27, n. 4, TC4009, http://dx.doi.org/10.1029/2007TC002116
Foley, S. F., 2008, Rejuvenation and erosion of the cratonic lithosphere: Nature Geoscience, v. 1, p. 503–510, http://dx.doi.org/10.1038/ngeo261
Frey, F. A., McNaughton, N. J., Nelson, D. R., deLaeter, J. R., and Duncan, R. A., 1996, Petrogenesis of the Bunbury Basalt, Western Australia: interaction between the Kerguelen plume and Gondwana lithosphere?: Earth and Planetary Science Letters, v. 144, n. 1–2, p. 163–183, http://dx.doi.org/10.1016/0012-821X(96)00150-1
Gallagher, K., and Hawkesworth, C., 1992, Dehydration melting and the generation of continental flood basalts: Nature, v. 358, p. 57–59, http://dx.doi.org/10.1038/358057a0
Gao, S., Luo, T. C., Zhang, B. R., Zhang, H. F., Han, Y. W., Zhao, Z. D., and Hu, Y. K., 1998, Chemical composition of the continental crust as revealed by studies in East China: Geochimica et Cosmochimica Acta, v. 62, n. 11, p. 1959–1975, http://dx.doi.org/10.1016/S0016-7037(98)00121-5
Garland, F., Turner, S., and Hawkesworth, C., 1996, Shifts in the source of the Paraná basalts through time: Lithos, v. 37, n. 2–3, p. 223–243, http://dx.doi.org/10.1016/0024-4937(95)00038-0
Ge, R. F., Zhu, W. B., Zheng, B. H., Wu, H. L., He, J. W., and Zhu, X. Q., 2012, Early Pan-African magmatism in the Tarim Craton: Insights from zircon U–Pb–Lu–Hf isotope and geochemistry of granitoids in the Korla area, NW China: Precambrian Research, v. 212–213, p. 117–138, http://dx.doi.org/10.1016/j.precamres.2012.05.001
Gibson, S. A., Thompson, R. N., Dickin, A. P., and Leonardos, O. H., 1995, High-Ti and low-Ti mafic potassic magmas: Key to plume-lithosphere interactions and continental flood-basalt genesis: Earth and Planetary Science Letters, v. 136, n. 3–4, p. 149–165, http://dx.doi.org/10.1016/0012-821X(95)00179-G
Gibson, S. A., Thompson, R. N., and Day, J. A., 2006, Timescales and mechanisms of plume–lithosphere interactions: $^{40}Ar/^{39}Ar$ geochronology and geochemistry of alkaline igneous rocks from the Paraná–Etendeka large igneous province: Earth and Planetary Science Letters, v. 251, n. 1–2, p. 1–17, http://dx.doi.org/10.1016/j.epsl.2006.08.004
Greenough, J. D., and Kyser, T. K., 2003, Contrasting Archean and Proterozoic lithospheric mantle: isotopic evidence from the Shonkin Sag sill (Montana): Contributions to Mineralogy and Petrology, v. 145, n. 2, p. 169–181, http://dx.doi.org/10.1007/s00410-002-0435-9
Greenough, J. D., Dostal, J., and Mallory-Greenough, L. M., 2005, Igneous rock associations 5. Oceanic island volcanism II: Mantle processes: Geoscience Canada, v. 32, n. 2, p. 77–90, http://dx.doi.org/10.12789/gs.v32i2.2703
——— 2007, Incompatible element ratios in French Polynesia basalts: describing mantle component fingerprints: Australian Journal of Earth Sciences, v. 54, n. 7, p. 947–958, http://dx.doi.org/10.1080/08120090701488271
Greenough, J. D., Kamo, S. L., Theny, L., Crowe, S. A., and Fipke, C., 2011, High-precision U-Pb age and geochemistry of the mineralized (Ni-Cu-Co) Suwar intrusion, Yemen: Canadian Journal of Earth Sciences, v. 48, n. 2, p. 495–514, http://dx.doi.org/10.1139/E10-067
Griffiths, R. W., and Campbell, I. H., 1990, Stirring and structure in mantle starting plumes: Earth and Planetary Science Letters, v. 99, n. 1–2, 66–78, http://dx.doi.org/10.1016/0012-821X(90)90071-5
Han, B. F., He, G. Q., Wang, X. C., and Guo, Z. J., 2011, Late Carboniferous collision between the Tarim and Kazakhstan–Yili terranes in the western segment of the South Tian Shan Orogen, Central Asia, and implications for the Northern Xinjiang, western China: Earth-Science Reviews, v. 109, n. 3–4, p. 74–93, http://dx.doi.org/10.1016/j.earscirev.2011.09.001
Hart, S. R., 1984, A large-scale isotope anomaly in the Southern Hemisphere mantle: Nature, v. 309, p. 753–757, http://dx.doi.org/10.1038/309753a0

Hart, S. R., and Dunn, T., 1993, Experimental cpx/melt partitioning of 24 trace elements: Contributions to Mineralogy and Petrology, v. 113, n. 1, p. 1–8, http://dx.doi.org/10.1007/BF00320827

He, B., Xu, Y. G., Chung, S. L., Xiao, L., and Wang, Y. M., 2003, Sedimentary evidence for a rapid, kilometer-scale crustal doming prior to the eruption of the Emeishan flood basalts: Earth and Planetary Science Letters, v. 213, n. 3–4, p. 391–405, http://dx.doi.org/10.1016/S0012-821X(03)00323-6

He, Z. Y., Zhang, Z. M., Zong, K. Q., Wang, W., and Santosh, M., 2012, Neoproterozoic granulites from the northeastern margin of the Tarim Craton: Petrology, zircon U–Pb ages and implications for the Rodinia assembly: Precambrian Research, v. 212–213, p. 21–33, http://dx.doi.org/10.1016/j.precamres.2012.04.014

Hellebrand, E., Snow, J. E., Hoppe, P., and Hofmann, A. W., 2002, Garnet-field melting and late-stage refertilization in "residual" abyssal peridotites from the Central Indian Ridge: Journal of Petrology, v. 43, n. 12, p. 2305–2338, http://dx.doi.org/10.1093/petrology/43.12.2305

Hergt, J. M., Peate, D. W., and Hawkesworth, C. J., 1991, The petrogenesis of Mesozoic Gondwana low-Ti flood basalts: Earth and Planetary Science Letters, v. 105, n. 1–3, p. 134–148, http://dx.doi.org/10.1016/0012-821X(91)90126-3

Hill, R. I., Campbell, I. H., Davies, G. F., and Griffiths, R. W., 1992, Mantle plumes and continental tectonics: Science, v. 256, n. 5054, p. 186–193, http://dx.doi.org/10.1126/science.256.5054.186

Hofmann, A. W., 2003, Sampling mantle heterogeneity through oceanic basalts: isotopes and trace elements, *in* Carlson, R. editor, Geochemistry of the Mantle and Core: Treatise on Geochemistry, v. 2, p. 61–101, http://dx.doi.org/10.1016/B0-08-043751-6/02123-X

Hofmann, A. W., Jochum, K. P., Seufert, M., and White, W. M., 1986, Nb and Pb in oceanic basalts: new constraints on mantle evolution: Earth and Planetary Science Letters, v. 79, n. 1–2, p. 33–45, http://dx.doi.org/10.1016/0012-821X(86)90038-5

Hofmann, C., Féraud, G., and Courtillot, V., 2000, $^{40}Ar/^{39}Ar$ dating of mineral separates and whole rocks from the Western Ghats lava pile: further constraints on duration and age of the Deccan traps: Earth and Planetary Science Letters, v. 180, n. 1–2, p. 13–27, http://dx.doi.org/10.1016/S0012-821X(00)00159-X

Hu, A. Q., Jahn, B. M., Zhang, G. X., Chen, Y. B., and Zhang, Q. F., 2000, Crustal evolution and Phanerozoic crustal growth in northern Xinjiang: Nd isotopic evidence. Part I. Isotopic characterization of basement rocks: Tectonophysics, v. 328, p. 15–51, http://dx.doi.org/10.1016/S0040-1951(00)00176-1

Huang, X. L., Xu, Y. G., and Liu, D. Y., 2004, Geochronology, petrology and geochemistry of the granulite xenoliths from Nushan, east China: Implication for a heterogeneous lower crust beneath the Sino-Korean Craton: Geochimica et Cosmochimica Acta, v. 68, n. 1, p. 127–149, http://dx.doi.org/10.1016/S0016-7037(03)00416-2

Huang, X. L., Niu, Y. L., Xu, Y. G., Ma, J. L., Qiu, H. N., and Zhong, J. W., 2013, Geochronology and geochemistry of Cenozoic basalts from eastern Guangdong, SE China: constraints on the lithosphere evolution beneath the northern margin of the South China Sea: Contributions to Mineralogy and Petrology, v. 165, n. 3, p. 437–455, http://dx.doi.org/10.1007/s00410-012-0816-7

Irvine, T. N., and Baragar, W. R. A., 1971, A guide to the chemical classification of the common volcanic rocks: Canadian Journal of Earth Sciences, v. 8, n. 5, p. 523–548, http://dx.doi.org/10.1139/e71-055

Jahn, B. M., Wu, F. Y., Lo, C. H., and Tsai, C. H., 1999, Crust–mantle interaction induced by deep subduction of the continental crust: geochemical and Sr–Nd isotopic evidence from post-collisional mafic–ultramafic intrusions of the northern Dabie complex, central China: Chemical Geology, v. 157, n. 1–2, p. 119–146, http://dx.doi.org/10.1016/S0009-2541(98)00197-1

Jiang, C. Y., Zhang, P. B., Lu, D. R., Bai, K. Y., Wang, Y. P., Tang, S. H., Wang, J. H., and Yang, C., 2004, Petrology, geochemistry and petrogenesis of the Kalpin basalts and their Nd, Sr and Pb isotopic compositions: Geological Review, v. 50, p. 492–500 (in Chinese with English abstract).

Jiang, N., Guo, J. H., and Chang, G. H., 2013, Nature and evolution of the lower crust in the eastern North China craton: A review: Earth-Science Reviews, v. 122, p. 1–9, http://dx.doi.org/10.1016/j.earscirev.2013.03.006

Johnson, M. C., and Plank, T., 2000, Dehydration and melting experiments constrain the fate of subducted sediments: Geochemistry Geophysics Geosystems, v. 1, n. 12, p. 1–26, http://dx.doi.org/10.1029/1999GC000014

Jones, D. L., Duncan, R. A., Briden, J. C., Randall, D. E., and MacNiocaill, C., 2001, Age of the Batoka basalts, northern Zimbabwe, and the duration of Karoo Large Igneous Province magmatism: Geochemistry Geophysics Geosystems, v. 2, n. 2, p. art.no.-2000GC000110, http://dx.doi.org/10.1029/2000GC000110

Jourdan, F., Bertrand, H., Schärer, U., Blichert-Toft, J., Féraud, G., and Kampunzu, A. B., 2007a, Major and trace element and Sr, Nd, Hf, and Pb isotope compositions of the Karoo large igneous province, Botswana–Zimbabwe: lithosphere vs mantle plume contribution: Journal of Petrology, v. 48, n. 6, p. 1043–1077, http://dx.doi.org/10.1093/petrology/egm010

Jourdan, F., Féraud, G., Bertrand, H., Watkeys, M. K., and Renne, P. R., 2007b, Distinct brief major events in the Karoo large igneous province clarified by new $^{40}Ar/^{39}Ar$ ages on the Lesotho basalts: Lithos, v. 98, n. 1–4, p. 195–209, http://dx.doi.org/10.1016/j.lithos.2007.03.002

Kamber, B. S., Greig, A., Schoenberg, R., and Collerson, K. D., 2003, A refined solution to Earth's hidden niobium: implications for evolution of continental crust and mode of core formation: Precambrian Research, v. 126, n. 3–4, p. 289–308, http://dx.doi.org/10.1016/S0301-9268(03)00100-1

Kamenetsky, V. S., Chung, S. L., Kamenetsky, M. B., and Kuzmin, D. V., 2012, Picrites from the Emeishan large igneous province, SW China: a compositional continuum in primitive magmas and their respective mantle sources: Journal of Petrology, v. 53, n. 10, p. 2095–2113, http://dx.doi.org/10.1093/petrology/egs045

Kaneoka, I., 1980, $^{40}Ar/^{39}Ar$ dating on volcanic rocks of the Deccan Traps, India: Earth and Planetary Science Letters, v. 46, n. 2, p. 233–243, http://dx.doi.org/10.1016/0012-821X(80)90009-6

Kinzler, R. J., 1997, Melting of mantle peridotite at pressures approaching the spinel to garnet transition: Application to mid-ocean ridge basalt petrogenesis: Journal of Geophysical Research-Solid Earth, v. 102, n. B1, p. 853–874, http://dx.doi.org/10.1029/96JB00988

Koppers, A. A. P., 2002, ArArCALC—software for $^{40}Ar/^{39}Ar$ age calculations: Computers & Geosciences, v. 28, n. 5, p. 605–619, http://dx.doi.org/10.1016/S0098-3004(01)00095-4

Kuang, Y. S., Wei, X., Hong, L. B., Ma, J. L., Pang, C. J., Zhong, Y. T., Zhao, J. X., and Xu, Y. G., 2012, Petrogenetic evaluation of the Laohutai basalts from North China Craton: Melting of a two-component source during lithospheric thinning in the late Cretaceous-early Cenozoic: Lithos, v. 154, p. 68–82, http://dx.doi.org/10.1016/j.lithos.2012.06.027

Le Bas, M. J., Le Maitre, R. W., Streckeisen, A., and Zanettin, B., 1986, A chemical classification of volcanic rocks based on the total alkali-silica diagram: Journal of Petrology, v. 27, n. 3, p. 745–750, http://dx.doi.org/10.1093/petrology/27.3.745

Lebedev, S., Meier, T., and van der Hilst, R. D., 2006, Asthenospheric flow and origin of volcanism in the Baikal Rift area: Earth and Planetary Science Letters, v. 249, n. 3–4, p. 415–424, http://dx.doi.org/10.1016/j.epsl.2006.07.007

Leeman, W. P., Ma, M. S., Murali, A. V., and Schmitt, R. A., 1978, Empirical estimation of magnetite-liquid distribution coefficients for some transition-elements: Contributions to Mineralogy and Petrology, v. 65, n. 3, p. 269–272, http://dx.doi.org/10.1007/BF00375512

Leeman, W. P., Menzies, M. A., Matty, D. J., and Embree, G. F., 1985, Strontium, neodymium and lead isotopic compositions of deep crustal xenoliths from the Snake River Plain: evidence for Archean basement: Earth and Planetary Science Letters, v. 75, n. 4, p. 354–368, http://dx.doi.org/10.1016/0012-821X(85)90179-7

Li, B. P., Greig, A., Zhao, J. X., Collerson, K. D., Quan, K. S., Meng, Y. H., and Ma, Z. L., 2005, ICP-MS trace element analysis of Song dynasty porcelains from Ding, Jiexiu and Guantai kilns, north China: Journal of Archaeological Science, v. 32, n. 2, p. 251–259, http://dx.doi.org/10.1016/j.jas.2004.09.004

Li, X. H., Li, Z. X., Wingate, M. T. D., Chung, S. L., Liu, Y., Lin, G. C., and Li, W. X., 2006, Geochemistry of the 755 Ma Mundine Well dyke swarm, northwestern Australia: Part of a Neoproterozoic mantle superplume beneath Rodinia?: Precambrian Research, v. 146, n. 1–2, p. 1–15, http://dx.doi.org/10.1016/j.precamres.2005.12.007

Li, Y., Su, W., Kong, P., Qian, Y. X., Zhang, K. Y., Zhang, M. L., Chen, Y., Cai, X. Y., and You, D. H., 2007, Zircon U-Pb ages of the early Permian magmatic rocks in the Tazhong-Bachu region, Tarim basin by LA-ICP-MS: Acta Petrologica Sinica, v. 23, n. 5, p. 1097–1107 (in Chinese with English abstract).

Li, Y. Q., Li, Z. L., Sun, Y. L., Santosh, M., Langmuir, C. H., Chen, H. L., Yang, S. F., Chen, Z. X., and Yu, X., 2012a, Platinum-group elements and geochemical characteristics of the Permian continental flood basalts in the Tarim Basin, northwest China: Implications for the evolution of the Tarim Large Igneous Province: Chemical Geology, v. 328, p. 278–289, http://dx.doi.org/10.1016/j.chemgeo.2012.03.007

Li, Z. L., Chen, H. L., Song, B. A., Li, Y. Q., Yang, S. F., and Yu, X., 2011, Temporal evolution of the Permian large igneous province in Tarim Basin in northwestern China: Journal of Asian Earth Sciences, v. 42, n. 5, p. 917–927, http://dx.doi.org/10.1016/j.jseaes.2011.05.009

Li, Z. L., Li, Y. Q., Chen, H. L., Santosh, M., Yang, S. F., Xu, Y. G., Langmuir, C. H., Chen, Z. X., Yu, X., and Zou, S. Y., 2012b, Hf isotopic characteristics of the Tarim Permian large igneous province rocks of NW China: Implication for the magmatic source and evolution: Journal of Asian Earth Sciences, v. 49, p. 191–202, http://dx.doi.org/10.1016/j.jseaes.2011.11.021

Li, Z. L., Yang, S. F., Chen, H. L., Langmuir, C. H., Yu, X., Lin, X. B., and Li, Y. Q., 2008, Chronology and geochemistry of Taxinan basalts from the Tarim basin: evidence for Permian plume magmatism: Acta Petrologica Sinica, v. 24, n. 5, p. 959–970 (in Chinese with English abstract).

Lightfoot, P. C., Hawkesworth, C. J., Hergt, J., Naldrett, A. J., Gorbachev, N. S., Fedorenko, V. A., and Doherty, W., 1993, Remobilisation of the continental lithosphere by a mantle plume: major-, trace-element, and Sr-, Nd-, and Pb-isotope evidence from picritic and tholeiitic lavas of the Noril'sk District, Siberian Trap, Russia: Contributions to Mineralogy and Petrology, v. 114, n. 2, p. 171–188, http://dx.doi.org/10.1007/BF00307754

Liou, J. G., Graham, S. A., Maruyama, S., and Zhang, R. Y., 1996, Characteristics and tectonic significance of the Late Proterozoic Aksu blueschists and diabasic dikes, northwest Xinjiang, China: International Geology Review, v. 38, n. 3, p. 228–244, http://dx.doi.org/10.1080/00206819709465332

Liu, S. W., Wang, L. S., Li, C., Li, H., Han, Y. B., Jia, C. Z., and Wei, G. Q., 2004, Thermal-rheological structure of lithosphere beneath the northern flank of Tarim Basin, western China: Implications for geodynamics: Science in China Series D-Earth Sciences, v. 47, n. 7, p. 659–672, http://dx.doi.org/10.1360/03yd0471

Liu, Y. S., Gao, S., Yuan, H. L., Zhou, L., Liu, X. M., Wang, X. C., Hu, Z. C., and Wang, L. S., 2004, U-Pb zircon ages and Nd, Sr, and Pb isotopes of lower crustal xenoliths from North China Craton: insights on evolution of lower continental crust: Chemical Geology, v. 211, n. 1–2, p. 87–109, http://dx.doi.org/10.1016/j.chemgeo.2004.06.023

Long, X. P., Yuan, C., Sun, M., Zhao, G. C., Xiao, W. J., Wang, Y. J., Yang, Y. H., and Hu, A. Q., 2010, Archean crustal evolution of the northern Tarim craton, NW China: Zircon U-Pb and Hf isotopic constraints: Precambrian Research, v. 180, n. 3–4, p. 272–284, http://dx.doi.org/10.1016/j.precamres.2010.05.001

Long, X. P., Yuan, C., Sun, M., Kröner, A., Zhao, G. C., Wilde, S., and Hu, A. Q., 2011, Reworking of the Tarim Craton by underplating of mantle plume-derived magmas: Evidence from Neoproterozoic granitoids in the Kuluketage area, NW China: Precambrian Research, v. 187, n. 1–2, p. 1–14, http://dx.doi.org/10.1016/j.precamres.2011.02.001

Lu, S. N., Zhao, G. C., Wang, H. C., and Hao, G. J., 2008, Precambrian metamorphic basement and sedimentary cover of the North China Craton: A review: Precambrian Research, v. 160, n. 1–2, p. 77–93, http://dx.doi.org/10.1016/j.precamres.2007.04.017

Lü, Z., Zhang, L. F., Du, J. X., and Bucher, K., 2008, Coesite inclusions in garnet from eclogitic rocks in western Tianshan, northwest China: Convincing proof of UHP metamorphism: American Mineralogist, v. 93, n. 11–12, p. 1845–1850, http://dx.doi.org/10.2138/am.2008.2800

Marini, J. C., Chauvel, C., and Maury, R., 2005, Hf isotope compositions of northern Luzon arc lavas suggest involvement of pelagic sediments in their source: Contributions to Mineralogy and Petrology, v. 149, n. 2, p. 216–232, http://dx.doi.org/10.1007/s00410-004-0645-4

Martin, E., Paquette, J. L., Bosse, V., Ruffet, G., Tiepolo, M., and Sigmarsson, O., 2011, Geodynamics of rift–plume interaction in Iceland as constrained by new $^{40}Ar/^{39}Ar$ and *in situ* U–Pb zircon ages: Earth and Planetary Science Letters, v. 311, n. 1–2, p. 28–38, http://dx.doi.org/10.1016/j.epsl.2011.08.036

McDonough, W. F., and Sun, S. S., 1995, The composition of the earth: Chemical Geology, v. 120, n. 3–4, p. 223–253, http://dx.doi.org/10.1016/0009-2541(94)00140-4

McKenzie, D., and O'Nions, R. K., 1991, Partial melt distribution from inversion of rare earth element concentrations: Journal of Petrology, v. 32, n. 5, p. 1021–1091, http://dx.doi.org/10.1093/petrology/32.5.1021

Míková, J., and Denková, P., 2007, Modified chromatographic separation scheme for Sr and Nd isotope analysis in geological silicate samples: Journal of Geosciences, v. 52, n. 3–4, p. 221–226, http://dx.doi.org/10.3190/jgeosci.015

Noll, P. D., Jr., Newsom, H. E., Leeman, W. P., and Ryan, J. G., 1996, The role of hydrothermal fluids in the production of subduction zone magmas: Evidence from siderophile and chalcophile trace elements and boron: Geochimica et Cosmochimica Acta, v. 60, n. 4, p. 587–611, http://dx.doi.org/10.1016/0016-7037(95)00405-X

Patchett, P. J., White, W. M., Feldmann, H., Kielinczuk, S., and Hofmann, A. W., 1984, Hafnium/rare earth element fractionation in the sedimentary system and crustal recycling into the Earth's mantle: Earth and Planetary Science Letters, v. 69, n. 2, p. 365–378, http://dx.doi.org/10.1016/0012-821X(84)90195-X

Peate, D. W., and Hawkesworth, C. J., 1996, Lithospheric to asthenospheric transition in Low-Ti flood basalts from southern Paraná, Brazil: Chemical Geology, v. 127, n. 1–3, p. 1–24, http://dx.doi.org/10.1016/0009-2541(95)00086-0

Peate, D. W., Hawkesworth, C. J., Mantovani, M. M. S., Rogers, N. W., and Turner, S. P., 1999, Petrogenesis and stratigraphy of the high-Ti/Y Urubici magma type in the Paraná flood basalt province and implications for the nature of "Dupal"-type mantle in the South Atlantic region: Journal of Petrology, v. 40, n. 3, p. 451–473, http://dx.doi.org/10.1093/petroj/40.3.451

Pin, C., and Zalduegui, J. S., 1997, Sequential separation of light rare-earth elements, thorium and uranium by miniaturized extraction chromatography: Application to isotopic analyses of silicate rocks: Analytica Chimica Acta, v. 339, n. 1–2, p. 79–89, http://dx.doi.org/10.1016/S0003-2670(96)00499-0

Pirajno, F., Mao, J. W., Zhang, Z. C., Zhang, Z. H., and Chai, F. M., 2008, The association of mafic–ultramafic intrusions and A-type magmatism in the Tian Shan and Altay orogens, NW China: Implications for geodynamic evolution and potential for the discovery of new ore deposits: Journal of Asian Earth Sciences, v. 32, n. 2–4, p. 165–183, http://dx.doi.org/10.1016/j.jseaes.2007.10.012

Plank, T., and Langmuir, C. H., 1998, The chemical composition of subducting sediment and its consequences for the crust and mantle: Chemical Geology, v. 145, n. 3–4, p. 325–394, http://dx.doi.org/10.1016/S0009-2541(97)00150-2

Priestley, K., Debayle, E., McKenzie, D., and Pilidou, S., 2006, Upper mantle structure of eastern Asia from multimode surface waveform tomography: Journal of Geophysical Research-Solid Earth, v. 111, n. B10, http://dx.doi.org/10.1029/2005JB004082

Qi, L., and Zhou, M. F., 2008, Platinum-group elemental and Sr-Nd-Os isotopic geochemistry of Permian Emeishan flood basalts in Guizhou Province, SW China: Chemical Geology, v. 248, n. 1–2, p. 83–103, http://dx.doi.org/10.1016/j.chemgeo.2007.11.004

Qin, K. Z., Su, B. X., Sakyi, P. A., Tang, D. M., Li, X. H., Sun, H., Xiao, Q. H., and Liu, P. P., 2011, SIMS zircon U-Pb geochronology and Sr-Nd isotopes of Ni-Cu-bearing mafic-ultramafic intrusions in eastern Tianshan and Beishan in correlation with flood basalts in Tarim Basin (NW China): constraints on a *ca.* 280 Ma mantle plume: American Journal of Science, v. 311, n. 3, p. 237–260, http://dx.doi.org/10.2475/03.2011.03

Qiu, H. N., and Wijbrans, J. R., 2008, The Paleozoic metamorphic history of the Central Orogenic Belt of China from $^{40}Ar/^{39}Ar$ geochronology of eclogite garnet fluid inclusions: Earth and Planetary Science Letters, v. 268, n. 3–4, p. 501–514, http://dx.doi.org/10.1016/j.epsl.2008.01.042

Reichow, M. K., Saunders, A. D., White, R. V., Pringle, M. S., Al'Mukhamedov, A. I., Medvedev, A. I., and Kirda, N. P., 2002, $^{40}Ar/^{39}Ar$ dates from the West Siberian Basin: Siberian flood basalt province doubled: Science, v. 296, p. 1846–1849, http://dx.doi.org/10.1126/science.1071671

Reichow, M. K., Pringle, M. S., Al'Mukhamedov, A. I., Allen, M. B., Andreichev, V. L., Buslov, M. M., Davies, C. E., Fedoseev, G. S., Fitton, J. G., Inger, S., Medvedev, A. Y., Mitchell, C., Puchkov, V. N., Safonova, I. Y., Scott, R. A., and Saunders, A. D., 2009, The timing and extent of the eruption of the Siberian Traps large igneous province: Implications for the end-Permian environmental crisis: Earth and Planetary Science Letters, v. 277, n. 1–2, p. 9–20, http://dx.doi.org/10.1016/j.epsl.2008.09.030

Renne, P. R., and Basu, A. R., 1991, Rapid eruption of the Siberian Traps flood basalts at the Permo–Triassic boundary: Science, v. 253, n. 5016, p. 176–179, http://dx.doi.org/10.1126/science.253.5016.176

Richards, M. A., Duncan, R. A., and Courtillot, V. E., 1989, Flood basalts and hot-spot tracks: Plume heads and tails: Science, v. 246, n. 4926, p. 103–107, http://dx.doi.org/10.1126/science.246.4926.103

Richards, M. A., Jones, D. L., Duncan, R. A., and Depaolo, D. J., 1991, A mantle plume initiation model for the Wrangellia flood basalt and other oceanic plateaus: Science, v. 254, n. 5029, p. 263–267, http://dx.doi.org/10.1126/science.254.5029.263

Rocha, E. R. V., Puchtel, I. S., Marques, L. S., Walker, R. J., Machado, F. B., Nardy, A. J. R., Babinski, M., and Figueiredo, A. M. G., 2012, Re-Os isotope and highly siderophile element systematics of the Paraná

continental flood basalts (Brazil): Earth and Planetary Science Letters, v. 337–338, p. 164–173, http://dx.doi.org/10.1016/j.epsl.2012.04.050

Rudnick, R. L., 1990, Nd and Sr isotopic compositions of lower crustal xenoliths from north Queensland, Australia: implications for Nd model ages and crustal growth processes: Chemical Geology, v. 83, n. 3–4, p. 195–208, http://dx.doi.org/10.1016/0009-2541(90)90280-K

Rudnick, R. L., and Gao, S., 2003, Composition of the continental crust, *in* Rudnick, R. L. editor, The Crust: Treatise on Geochemistry, v. 3, p. 1–64, http://dx.doi.org/10.1016/B0-08-043751-6/03016-4

Rudnick, R. L., McDonough, W. F., McCulloch, M. T., and Taylor, S. R., 1986, Lower crustal xenoliths from Queensland, Australia: Evidence for deep crustal assimilation and fractionation of continental basalts: Geochimica et Cosmochimica Acta, v. 50, n. 6, p. 1099–1115, http://dx.doi.org/10.1016/0016-7037(86)90391-1

Salters, V. J. M., and Sachi-Kocher, A., 2010, An ancient metasomatic source for the Walvis Ridge basalts: Chemical Geology, v. 273, n. 3–4, p. 151–167, http://dx.doi.org/10.1016/j.chemgeo.2010.02.010

Sebai, A., Zumbo, V., Féraud, G., Bertrand, H., Hussain, A. G., Giannérini, G., and Campredon, R., 1991, $^{40}Ar/^{39}Ar$ dating of alkaline and tholeiitic magmatism of Saudi Arabia related to the early Red Sea Rifting: Earth and Planetary Science Letters, v. 104, n. 2–3, p. 473–487, http://dx.doi.org/10.1016/0012-821X(91)90223-5

Shangguan, S. M., Tian, W., Li, X. H., Guan, P., Pan, M., Chen, M. M., and Pan, W. Q., 2011, SIMS zircon U-Pb age of a rhyolite layer from the Halahatang area, Northern Tarim, NW China: constraint on the eruption age of major pulse of Tarim flood basalt: Acta Scientiarum Naturalium Universitatis Pekinensis, v. 47, n. 3, p. 561–564 (in Chinese with English abstract).

Shaw, D. M., 1970, Trace element fractionation during anatexis: Geochimica et Cosmochimica Acta, v. 34, n. 2, p. 237–243, http://dx.doi.org/10.1016/0016-7037(70)90009-8

Shellnutt, J. G., and Jahn, B. M., 2010, Formation of the Late Permian Panzhihua plutonic-hypabyssal-volcanic igneous complex: Implications for the genesis of Fe–Ti oxide deposits and A-type granites of SW China: Earth and Planetary Science Letters, v. 289, n. 34, p. 509–519, http://dx.doi.org/10.1016/j.epsl.2009.11.044

Shellnutt, J. G., and Zhou, M. F., 2007, Permian peralkaline, peraluminous and metaluminous A-type granites in the Panxi district, SW China: Their relationship to the Emeishan mantle plume: Chemical Geology, v. 243, n. 3–4, p. 286–316, http://dx.doi.org/10.1016/j.chemgeo.2007.05.022

Shomali, Z. H., Roberts, R. G., Pedersen, L. B., and the TOW Working Group, 2006, Lithospheric structure of the Tornquist Zone resolved by nonlinear P and S teleseismic tomography along the TOR array: Tectonophysics, v. 416, n. 1–4, p. 133–149, http://dx.doi.org/10.1016/j.tecto.2005.11.019

Sleep, N. H., Ebinger, C. J., and Kendall, J. M., 2002, Deflection of mantle plume material by cratonic keels, *in* Fowler, C. M. R., Ebinger, C. J., and Hawkesworth, C. J., editors, Early Earth: Physical, Chemical and Biological Development: Geological Society, London, Special Publications, v. 199, p. 135–150, 10.1144/GSL.SP.2002.199.01.08

Storey, M., Mahoney, J. J., and Saunders, A. D., 1997, Cretaceous basalts in Madagascar and the transition between plume and continental lithosphere mantle sources, *in* Maphoney, J. J., and Coffin, M. F., editors, Large igneous provinces: continental, oceanic, and planetary food volcanism: Geophysical Monograph Series, v. 100, p. 95–122, http://dx.doi.org/10.1029/GM100p0095

Su, B., Qin, K., Sakyi, P. A., Tang, D., Liu, P., Malaviarachchi, S. P. K., Xiao, Q., and Sun, H., 2012, Geochronologic-petrochemical studies of the Hongshishan mafic-ultramafic intrusion, Beishan area, Xinjiang (NW China): petrogenesis and tectonic implications: International Geology Review, v. 54, n. 3, p. 270–289, http://dx.doi.org/10.1080/00206814.2010.543011

Sun, S. S., and McDonough, W. F., 1989, Chemical and isotopic systematics of oceanic basalts: implications for mantle composition and processes: Geological Society, London, Special Publications, v. 42, p. 313–345, http://dx.doi.org/10.1144/GSL.SP.1989.042.01.19

Tanaka, T., Togashi, S., Kamioka, H., Amakawa, H., Kagami, H., Hamamoto, T., Yuhara, M., Orihashi, Y., Yoneda, S., Shimizu, H., Kunimaru, T., Takahashi, K., Yanagi, T., Nakano, T., Fujimaki, H., Shinjo, R., Asahara, Y., Tanimizu, M., and Dragusanu, C., 2000, JNdi-1: a neodymium isotopic reference in consistency with LaJolla neodymium: Chemical Geology, v. 168, n. 3–4, p. 279–281, http://dx.doi.org/10.1016/S0009-2541(00)00198-4

Tian, W., Campbell, I. H., Allen, C. M., Guan, P., Pan, W. Q., Chen, M. M., Yu, H. J., and Zhu, W. P., 2010, The Tarim picrite-basalt-rhyolite suite, a Permian flood basalt from northwest China with contrasting rhyolites produced by fractional crystallization and anatexis: Contributions to Mineralogy and Petrology, v. 160, n. 3, p. 407–425, http://dx.doi.org/10.1007/s00410-009-0485-3

Turner, S., and Hawkesworth, C., 1995, The nature of the sub-continental mantle: constraints from the major-element composition of continental flood basalts: Chemical Geology, v. 120, n. 3–4, p. 295–314, http://dx.doi.org/10.1016/0009-2541(94)00143-V

Turner, S., Hawkesworth, C., Gallagher, K., Stewart, K., Peate, D., and Mantovani, M., 1996, Mantle plumes, flood basalts, and thermal models for melt generation beneath continents: Assessment of a conductive heating model and application to the Paraná: Journal of Geophysical Research-Solid Earth, v. 101, n. B5, p. 11503–11518, http://dx.doi.org/10.1029/96JB00430

Vervoort, J. D., Patchett, P. J., Blichert-Toft, J., and Albarède, F., 1999, Relationships between Lu–Hf and Sm–Nd isotopic systems in the global sedimentary system: Earth and Planetary Science Letters, v. 168, n. 1–2, p. 79–99, http://dx.doi.org/10.1016/S0012-821X(99)00047-3

Vervoort, J. D., Plank, T., and Prytulak, J., 2011, The Hf–Nd isotopic composition of marine sediments: Geochimica et Cosmochimica Acta, v. 75, n. 20, p. 5903–5926, http://dx.doi.org/10.1016/j.gca.2011.07.046

Wei, X., and Xu, Y. G., 2011, Petrogenesis of Xiaohaizi syenite complex from Bachu area, Tarim: Acta Petrologica Sinica, v. 27, p. 2984–3004 (in Chinese with English abstract).

White, R., and McKenzie, D., 1989, Magmatism at rift zones: The generation of volcanic continental margins and flood basalts: Journal of Geophysical Research-Solid Earth and Planets, v. 94, n. B6, p. 7685–7729, http://dx.doi.org/10.1029/JB094iB06p07685

Willbold, M., and Stracke, A., 2006, Trace element composition of mantle end-members: Implications for recycling of oceanic and upper and lower continental crust: Geochemistry Geophysics Geosystems, v. 7, n. 4, http://dx.doi.org/10.1029/2005GC001005

Winchester, J. A., and Floyd, P. A., 1977, Geochemical discrimination of different magma series and their differentiation products using immobile elements: Chemical Geology, v. 20, p. 325–343, http://dx.doi.org/10.1016/0009-2541(77)90057-2

Wolfe, C. J., Solomon, S. C., Laske, G., Collins, J. A., Detrick, R. S., Orcutt, J. A., Bercovici, D., and Hauri, E. H., 2009, Mantle shear-wave velocity structure beneath the Hawaiian hot spot: Science, v. 326, n. 5958, p. 1388–1390, http://dx.doi.org/10.1126/science.1180165

Woodhead, J. D., Hergt, J. M., Davidson, J. P., and Eggins, S. M., 2001, Hafnium isotope evidence for "conservative" element mobility during subduction zone processes: Earth and Planetary Science Letters, v. 192, n. 3, p. 331–346, http://dx.doi.org/10.1016/S0012-821X(01)00453-8

Wu, X. Y., Sun, B. N., Shen, G. L., and Wang, Y. D., 1997, Permian fossil plants from northern margin of Tarim Basin, Xinjiang: Acta Palaeontologica Sinica, v. 36, p. 1–28 (in Chinese with English abstract).

Xiao, L., Xu, Y. G., Mei, H. J., Zheng, Y. F., He, B., and Pirajno, F., 2004, Distinct mantle sources of low-Ti and high-Ti basalts from the western Emeishan large igneous province, SW China: implications for plume-lithosphere interaction: Earth and Planetary Science Letters, v. 228, n. 3–4, p. 525–546, http://dx.doi.org/10.1016/j.epsl.2004.10.002

XIGMR (Xi'an Institute of Geology and Mineral Resources), 2007, Geological map of the Chinese Tianshan and adjacent regions: Geological Publishing House, scale 1:1,000,000.

Xu, B., Jian, P., Zheng, H. F., Zou, H. B., Zhang, L. F., and Liu, D. Y., 2005, U-Pb zircon geochronology and geochemistry of Neoproterozoic volcanic rocks in the Tarim Block of northwest China: implications for the breakup of Rodinia supercontinent and Neoproterozoic glaciations: Precambrian Research, v. 136, n. 2, p. 107–123, http://dx.doi.org/10.1016/j.precamres.2004.09.007

Xu, B., Xiao, S., Zou, H., Chen, Y., Li, Z. X., Song, B., Liu, D., Zhou, C., and Yuan, X., 2009, SHRIMP zircon U-Pb age constraints on Neoproterozoic Quruqtagh diamictites in NW China: Precambrian Research, v. 168, n. 3–4, p. 247–258, http://dx.doi.org/10.1016/j.precamres.2008.10.008

Xu, J. F., Suzuki, K., Xu, Y. G., Mei, H. J., and Li, J., 2007, Os, Pb, and Nd isotope geochemistry of the Permian Emeishan continental flood basalts: Insights into the source of a large igneous province: Geochimica et Cosmochimica Acta, v. 71, n. 8, p. 2104–2119, http://dx.doi.org/10.1016/j.gca.2007.01.027

Xu, Y. G., 2001, Thermo-tectonic destruction of the archaean lithospheric keel beneath the Sino-Korean Craton in China: Evidence, timing and mechanism: Physics and Chemistry of the Earth Part a-Solid Earth and Geodesy, v. 26, n. 9–10, p. 747–757, http://dx.doi.org/10.1016/S1464-1895(01)00124-7

Xu, Y. G., Chung, S. L., Jahn, B. M., and Wu, G. Y., 2001, Petrologic and geochemical constraints on the petrogenesis of Permian–Triassic Emeishan flood basalts in southwestern China: Lithos, v. 58, n. 3–4, p. 145–168, http://dx.doi.org/10.1016/S0024-4937(01)00055-X

Xu, Y. G., He, B., Chung, S. L., Menzies, M. A., and Frey, F. A., 2004a, Geologic, geochemical, and geophysical consequences of plume involvement in the Emeishan flood-basalt province: Geology, v. 32, n. 10, p. 917–920, http://dx.doi.org/10.1130/G20602.1

Xu, Y. G., Huang, X. L., Ma, J. L., Wang, Y. B., Iizuka, Y., Xu, J. F., Wang, Q., and Wu, X. Y., 2004b, Crust-mantle interaction during the tectono-thermal reactivation of the North China Craton: constraints from SHRIMP zircon U–Pb chronology and geochemistry of Mesozoic plutons from western Shandong: Contributions to Mineralogy and Petrology, v. 147, n. 6, p. 750–767, http://dx.doi.org/10.1007/s00410-004-0594-y

Yamasaki, S., Sawada, R., Ozawa, A., Tagami, T., Watanabe, Y., and Takahashi, E., 2011, Unspiked K–Ar dating of Koolau lavas, Hawaii: Evaluation of the influence of weathering/alteration on age determinations: Chemical Geology, v. 287, n. 1–2, p. 41–53, http://dx.doi.org/10.1016/j.chemgeo.2011.05.003

Yang, S. F., Chen, H. L., Dong, C. W., Jia, C. Z., and Wang, Z. G., 1996, The discovery of Permian syenite inside Tarim basin and its geodynamic significance: Geochimica, v. 25, p. 121–128 (in Chinese with English abstract).

Yang, S. F., Li, Z. L., Chen, H. L., Chen, W., and Yu, X., 2006a, ^{40}Ar-^{39}Ar dating of basalts from Tarim Basin, NW China and its implication to a Permian thermal tectonic event: Journal of Zhejiang University-Science A, v. 7, p. 320–324.

Yang, S. F., Li, Z. L., Chen, H. L., Xiao, W. J., Yu, X., Lin, X. B., and Shi, X. G., 2006b, Discovery of a Permian quartz syenitic porphyritic dyke from the Tarim basin and its tectonic implications: Acta Petrologica Sinica, v. 22, p. 1405–1412 (in Chinese with English abstract).

Yang, S. F., Li, Z. L., Chen, H. L., Santosh, M., Dong, C. W., and Yu, X., 2007, Permian bimodal dyke of Tarim Basin, NW China: Geochemical characteristics and tectonic implications: Gondwana Research, v. 12, n. 1–2, p. 113–120, http://dx.doi.org/10.1016/j.gr.2006.10.018

Yang, W., and Li, S. G., 2008, Geochronology and geochemistry of the Mesozoic volcanic rocks in Western Liaoning: Implications for lithospheric thinning of the North China Craton: Lithos, v. 102, n. 1–2, p. 88–117, http://dx.doi.org/10.1016/j.lithos.2007.09.018

Yu, J. C., Mo, X. X., Dong, G. C., Yu, X. H., Xing, F. C., Li, Y., and Huang, X. K., 2011a, Felsic volcanic rocks from northern Tarim, NW China: Zircon U-Pb dating and geochemical characteristics: Acta Petrologica Sinica, v. 27, p. 2184–2194 (in Chinese with English abstract).

Yu, X., ms, 2009, Magma evolution and deep geological processes of early Permian Tarim large igneous province: Hangzhou, Zhejiang University, Ph. D. thesis, 130 p. (in Chinese with English abstract).

Yu, X., Chen, H. L., Yang, S. F., Li, Z. L., Wang, Q. H., and Li, Z. H., 2010, Distribution characters of Permian

basalts and their geological significance in the Kalpin area, Xinjiang: Journal of Stratigraphy, v. 34, p. 127–134 (in Chinese with English abstract).
Yu, X., Yang, S. F., Chen, H. L., Chen, Z. Q., Li, Z. L., Batt, G. E., and Li, Y. Q., 2011b, Permian flood basalts from the Tarim Basin, Northwest China: SHRIMP zircon U-Pb dating and geochemical characteristics: Gondwana Research, v. 20, p. 485–497, http://dx.doi.org/10.1016/j.gr.2010.11.009
Zhang, C. L., Li, X. H., Li, Z. X., Lu, S. N., Ye, H. M., and Li, H. M., 2007, Neoproterozoic ultramafic-mafic-carbonatite complex and granitoids in Quruqtagh of northeastern Tarim Block, western China: Geochronology, geochemistry and tectonic implications: Precambrian Research, v. 152, n. 3–4, p. 149–169, http://dx.doi.org/10.1016/j.precamres.2006.11.003
Zhang, C. L., Li, X. H., Li, Z. X., Ye, H. M., and Li, C. N., 2008a, A Permian layered intrusive complex in the western Tarim Block, northwestern China: Product of a *Ca.* 275 Ma mantle plume?: The Journal of Geology, v. 116, n. 3, p. 269–287, http://dx.doi.org/10.1086/587726
Zhang, C. L., Li, Z. X., Li, X. H., and Ye, H. M., 2009a, Neoproterozoic mafic dyke swarms at the northern margin of the Tarim Block, NW China: Age, geochemistry, petrogenesis and tectonic implications: Journal of Asian Earth Sciences, v. 35, n. 2, p. 167–179, http://dx.doi.org/10.1016/j.jseaes.2009.02.003
Zhang, C. L., Li, Z. X., Li, X. H., Xu, Y. G., Zhou, G., and Ye, H. M., 2010a, A Permian large igneous province in Tarim and Central Asian orogenic belt, NW China: Results of a *ca.* 275 Ma mantle plume?: Geological Society of America Bulletin, v. 122, n. 11–12, p. 2020–2040, http://dx.doi.org/10.1130/B30007.1
Zhang, C. L., Xu, Y. G., Li, Z. X., Wang, H. Y., and Ye, H. M., 2010b, Diverse Permian magmatism in the Tarim Block, NW China: Genetically linked to the Permian Tarim mantle plume?: Lithos, v. 119, n. 3–4, p. 537–552, http://dx.doi.org/10.1016/j.lithos.2010.08.007
Zhang, C. L., Yang, D. S., Wang, H. Y., Takahashi, Y., and Ye, H. M., 2011, Neoproterozoic mafic-ultramafic layered intrusion in Quruqtagh of northeastern Tarim Block, NW China: Two phases of mafic igneous activity with different mantle sources: Gondwana Research, v. 19, n. 1, p. 177–190, http://dx.doi.org/10.1016/j.gr.2010.03.012
Zhang, C. L., Li, H. K., Santosh, M., Li, Z. X., Zou, H. B., Wang, H. Y., and Ye, H. M., 2012a, Precambrian evolution and cratonization of the Tarim Block, NW China: Petrology, geochemistry, Nd-isotopes and U–Pb zircon geochronology from Archaean gabbro-TTG–potassic granite suite and Paleoproterozoic metamorphic belt: Journal of Asian Earth Sciences, v. 47, p. 5–20, http://dx.doi.org/10.1016/j.jseaes.2011.05.018
Zhang, C. L., Zou, H. B., Li, H. K., and Wang, H. Y., 2013, Tectonic framework and evolution of the Tarim Block in NW China: Gondwana Research, v. 23, n. 4, p. 1306–1315, http://dx.doi.org/10.1016/j.gr.2012.05.009
Zhang, D. Y., Zhou, T. F., Yuan, F., Jowitt, S. M., Fan, Y., and Liu, S., 2012b, Source, evolution and emplacement of Permian Tarim Basalts: Evidence from U–Pb dating, Sr–Nd–Pb–Hf isotope systematics and whole rock geochemistry of basalts from the Keping area, Xinjiang Uygur Autonomous region, northwest China: Journal of Asian Earth Sciences, v. 49, p. 175–190, http://dx.doi.org/10.1016/j.jseaes.2011.10.018
Zhang, H. A., Li, Y. J., Wu, G. Y., Su, W., Qian, Y. X., Meng, Q. L., Cai, X. Y., Han, L. J., Zhao, Y., and Liu, Y. L., 2009b, Isotopic geochronology of Permian igneous rocks in the Tarim Basin: Chinese Journal of Geology, v. 44, p. 137–158 (in Chinese with English abstract).
Zhang, Y. T., Liu, J. Q., and Guo, Z. F., 2010c, Permian basaltic rocks in the Tarim basin, NW China: Implications for plume-lithosphere interaction: Gondwana Research, v. 18, n. 4, p. 596–610, http://dx.doi.org/10.1016/j.gr.2010.03.006
Zhang, Z. C., Mahoney, J. J., Mao, J. W., and Wang, F. S., 2006, Geochemistry of picritic and associated basalt flows of the western Emeishan flood basalt province, China: Journal of Petrology, v. 47, n. 10, p. 1997–2019, http://dx.doi.org/10.1093/petrology/egl034
Zhang, Z. L., Qin, Q. M., Tian, W., Cao, B., Li, B. S., and Chen, M. M., 2008b, Emplacement characteristics and spatial distribution of Permian Mazhartager basic dike swarms in Bachu area, Tarim basin: Acta Petrologica Sinica, v. 24, p. 2273–2280 (in Chinese with English abstract).
Zhao, Z. F., Zheng, Y. F., Zhang, J., Dai, L. Q., Li, Q. L., and Liu, X. M., 2012, Syn-exhumation magmatism during continental collision: Evidence from alkaline intrusives of Triassic age in the Sulu orogen: Chemical Geology, v. 328, p. 70–88, http://dx.doi.org/10.1016/j.chemgeo.2011.11.002
Zheng, T. Y., Zhao, L., Xu, W. W., and Zhu, R. X., 2008, Insight into modification of North China Craton from seismological study in the Shandong Province: Geophysical Research Letters, v. 35, n. 22, L22305, http://dx.doi.org/10.1029/2008GL035661
Zheng, Y. F., 2012, Metamorphic chemical geodynamics in continental subduction zones: Chemical Geology, v. 328, p. 5–48, http://dx.doi.org/10.1016/j.chemgeo.2012.02.005
Zheng, Y. F., Chen, R. X., and Zhao, Z. F., 2009, Chemical geodynamics of continental subduction-zone metamorphism: Insights from studies of the Chinese Continental Scientific Drilling (CCSD) core samples: Tectonophysics, v. 475, n. 2, p. 327–358, http://dx.doi.org/10.1016/j.tecto.2008.09.014
Zhong, H., Zhu, W. G., Chu, Z. Y., He, D. F., and Song, X. Y., 2007, Shrimp U–Pb zircon geochronology, geochemistry, and Nd–Sr isotopic study of contrasting granites in the Emeishan large igneous province, SW China: Chemical Geology, v. 236, n. 1–2, p. 112–133, http://dx.doi.org/10.1016/j.chemgeo.2006.09.004
Zhong, H., Campbell, I. H., Zhu, W. G., Allen, C. M., Hu, R. Z., Xie, L. W., and He, D. F., 2011, Timing and source constraints on the relationship between mafic and felsic intrusions in the Emeishan large igneous province: Geochimica et Cosmochimica Acta, v. 75, n. 5, p. 1374–1395, http://dx.doi.org/10.1016/j.gca.2010.12.016
Zhong, Y. T., and Xu, Y. G., 2009, Characteristics of plume-related A-type granites: an example from the Emeishan large igneous province: Journal of Jilin University (Earth Science Edition), v. 39, p. 828–838.
Zhou, M. F., Malpas, J., Song, X. Y., Robinson, P. T., Sun, M., Kennedy, A. K., Lesher, C. M., and Keays, R. R.,

2002, A temporal link between the Emeishan large igneous province (SW China) and the end-Guadalupian mass extinction: Earth and Planetary Science Letters, v. 196, n. 3–4, p. 113–122, http://dx.doi.org/10.1016/S0012-821X(01)00608-2

Zhou, M. F., Zhao, J. H., Jiang, C. Y., Gao, J. F., Wang, W., and Yang, S. H., 2009, OIB-like, heterogeneous mantle sources of Permian basaltic magmatism in the western Tarim Basin, NW China: Implications for a possible Permian large igneous province: Lithos, v. 113, n. 3–4, p. 583–594, http://dx.doi.org/10.1016/j.lithos.2009.06.027

Zhu, W. B., Zheng, B. H., Shu, L. S., Ma, D. S., Wu, H. L., Li, Y. X., Huang, W. T., and Yu, J. J., 2011, Neoproterozoic tectonic evolution of the Precambrian Aksu blueschist terrane, northwestern Tarim, China: Insights from LA-ICP-MS zircon U-Pb ages and geochemical data: Precambrian Research, v. 185, n. 3–4, p. 215–230, http://dx.doi.org/10.1016/j.precamres.2011.01.012

Zindler, A., and Hart, S., 1986, Chemical geodynamics: Annual Reviews of Earth and Planetary Sciences, v. 14, p. 493–571, http://dx.doi.org/10.1146/annurev.ea.14.050186.002425